Master's thesis
Master's Degree Programme in Physical Sciences

From analog to digital magnetometers: DigiMAG digitization and CubeMAG magnetometer concepts

Mika Väänänen
2019

Advisors: Eija Tanskanen, Jouni Envall
Examiners: Edward Haeggström, Eija Tanskanen

UNIVERSITY OF HELSINKI
DEPARTMENT OF PHYSICS

PL 64 (Gustaf Hällströmin katu 2)
00014 Helsingin yliopisto

HELSINGIN YLIOPISTO
HELSINGFORS UNIVERSITET
UNIVERSITY OF HELSINKI

Tiedekunta/Osasto Fakultet/Sektion – Faculty Matemaatis-luonnontieteellinen tiedekunta	Laitos/Institution– Department Fysiikan osasto	
Tekijä/Författare – Author Mika Väänänen		
Työn nimi / Arbetets titel – Title From analog to digital magnetometers: DigiMAG digitization and CubeMAG magnetometer concepts		
Oppiaine /Läroämne – Subject Fysikaaliset tieteet		
Työn laji/Arbetets art – Level Pro gradu	Aika/Datum – Month and year Kesäkuu 2019	Sivumäärä/ Sidoantal – Number of pages 49

Tiivistelmä/Referat – Abstract

For millennia, phenomena of the magnetosphere have intrigued mankind. Studies of the geomagnetic field were first initiated to locate precious minerals, later on continued for purposes of navigation and in the modern times for scientific interest and protection of modern society. Strong changes in the interplanetary magnetic field and pulses of charged particles originating from the Sun pose serious risks to many cornerstones of our lifestyle, such as the power grid, telecommunication and space safety. Understanding the interaction between the interplanetary magnetic field, solar wind and the geomagnetic field is crucial in building protection systems for these critical technologies. Magnetometers are practically the only instrument to monitor changed in the magnetic environment and thus a key instrument in broadening this understanding.

In this thesis I describe two projects: development of a digitization algorithm for old, analog magnetometer data and the design and building process of two small magnetometers: one for ground based measurements and one for space applications.

The aim of the digitization project was to digitize a magnetic timeseries produced in 1970s and 1980s. The quality of the dataset is very high, but since the data is saved on photographic film as graphs, proper time series analysis is difficult. During the project, I used a custom-made film scanner and developed a MATLAB program to read out the measured values from the scanned films.

The aim of the magnetometer building project was to show that it is possible to build science grade magnetometers from commercial-off-the-shelf (COTS) components, enabling magnetometric campaigns where state of the art instruments would be prohibitively expensive. One magnetometer was built based on the Honeywell HMC5883L sensor, controlled by a Raspberry Pi miniature computer. This magnetometer was placed at the Metsähovi Radio Observatory. Another magnetometer, the CubeMAG, was based on the Honeywell HMC2003 sensor and controlled by an STM32F100 microcontroller. This magnetometer will be one of the science payloads of the ESTCube-2 satellite.

The magnetometer placed in Metsähovi showed promising results, recording one strong geomagnetic storm which was also recorded with observatory quality instruments at the Nurmijärvi geophysical observatory. The resolution of the HMC5883L was too low to record most interesting features of the storm, but was high enough to show that the Metsähovi observatory is a suitable place for a more sensitive magnetometer.

As of writing this thesis, ESTCube-2 is in development and preparing for launch and scientific results from the CubeMAG are not available. Initial laboratory tests show promising results, with the significantly higher resolution of the HMC2003 compared to the HMC5883L being able to record very small changes in the surrounding magnetic field.

Avainsanat – Nyckelord – Keywords

Säilytyspaikka – Förvaringställe – Where deposited

Muita tietoja – Övriga uppgifter – Additional information

Contents

1 Introduction

Humankind has been interested in measuring magnetic fields since ancient times. Already in ancient Greece, 800BC, philosophers wrote about the strange properties of lodestone (a magnetic mineral). A few centuries later, in 300BC in China, the same material was used to manufacture the first compasses. These early instruments were not used for navigation but for finding gems and locating appropriate places for houses. Before 1000AD a compass was developed for navigation. Later on, different magnetometric instruments were developed for seismic measurements and even later, for space weather applications. [1]

Magnetic fields give us interesting information about the structure of the Universe itself: after all, over 99% of the Universe consists of plasma, movement of which is determined by magnetic fields. Earth's immediate vicinity is full of plasma and its dynamics are wholly determined by magnetic fields. The phenomena rising from the interaction of this plasma and Sun-Earth magnetic coupling affect electrical equipment on the surface of our planet and also satellites in the orbit, possibly causing economical damage reaching up to hundreds of millions of dollars. For example, the ADEOS-2 was destroyed in an exceptionally strong magnetic storm in 2003. The satellite was meant to produce data for climate change studies, but was destroyed before even starting its measurements. The same storm also caused 30 other significant satellite anomalies, including destroyed instruments, such as LEMS on-board the ACE satellite.

Magnetic phenomena at the near-Earth space pose serious health risks to astronauts. The radiation environment around Earth is very harsh, and can be made even more dangerous by disturbances in the interplanetary magnetic field and the geomagnetic field. Ability to detect, and possibly predict, these disturbances, would make space travel much safer.

In March 1989, a strong magnetic storm caused the power grid in Quebec, Canada, to black out for 9 hours. This resulted in loss of electricity for 6 million people. Losses for the power company totaled roughly C$13.2 million (10 million euros). The very same storm destroyed a transformer in a nuclear power plant, which caused an interruption in electricity production [2]. Other industries are also at risk: magnetic storms can induce high potentials and currents in gas and oil pipelines, disturbing monitoring systems and accelerating corrosion of the pipe material [3].

Studying magnetic phenomena of heliosphere and magnetosphere is the best way to predict these kind of catastrophic events and prepare for them. Unfortunately, scientific quality instruments are often very expensive, sometimes even prohibitively so. For this reason, the aim of this thesis is to describe the design and manufacturing processes of affordable instruments based on commercial off-the-shelf (COTS) components and modules. Such instruments usually do not perform quite as well as readymade, state of the art instruments, but their cost is usually an order of magnitude or two lower. Thus, COTS magnetometers can be used to for example try out a possible location for a new magnetometer station before investing thousands or tens of thousands of euros in a new, top grade magnetometer.

2 Background

2.1 Phenomena of the magnetosphere

The Earth's magnetic field is a relatively weak (in the order of $50 \cdot 10^3$ nanoteslas) field originating in the Earth's liquid core, roughly at a depth of 2900 kilometers. [4] There are strong electric currents in the core, produced by the flow of conducting fluids inside the core. These currents produce the planetary magnetic field. This process is called the dynamo and it is undergoing constant change. These changes cause the magnetic field on the surface to change in intensity and direction. The timescale of such variations ranges from days to decades and is called secular variation.

The terrestrial magnetic field is also strongly affected by the interplanetary magnetic field (IMF) which originates from the Sun. Changes in the IMF, caused by events in the Sun like Alfvén waves [Tanskanen et al 2017a], flares and coronal mass ejections [5], bring with them large amounts of charged particles to the near-Earth space and ionosphere. When these particles hit the magnetosphere of the Earth, they form currents in the magnetosphere and thus introduce another source of variation. These variations are short in duration, usually ranging from seconds to a single day and are seen as auroral substorms and pulsations in ground magnetic data. These short changes, called transient variations, are primarily caused by changes in solar wind [Tanskanen et al., 2002; Tanskanen et al., 2017b]. Figs. 1 and 2 show a clear magnetic substorm and Fig. 3 shows a record of geomagnetic pulsations. Transient variations give us information on space weather conditions, so observing them is of great interest when planning and

designing space flight missions. Transient variations also tell us about long-term variability of space weather, ie. space climate, which is changes in the plasma conditions in a timescale of decades to centuries. This thesis will focus more on instruments designed for space weather applications and therefore will cover instruments designed for measuring transient variations.

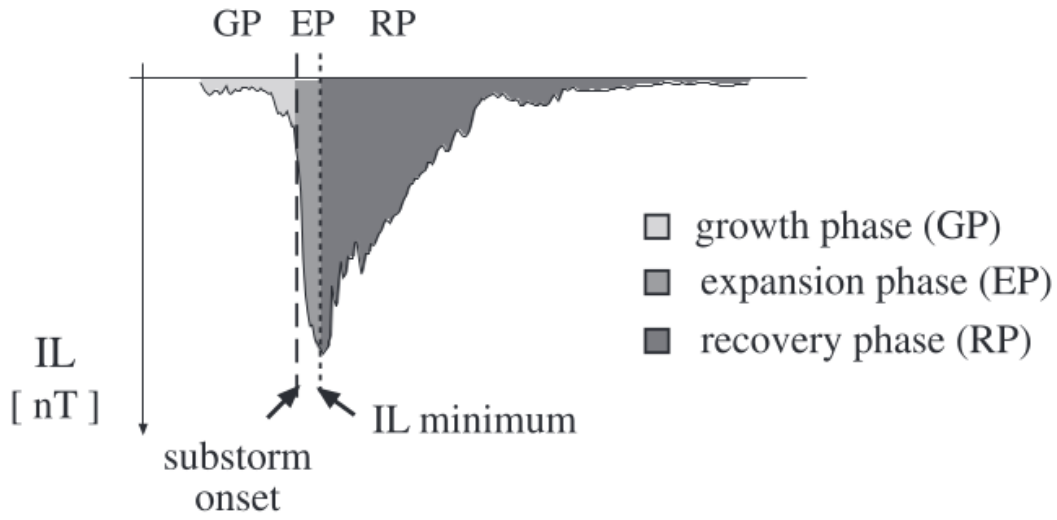

Figure 1: A sketch showing the time structure of a magnetic substorm. The horizontal axis shows time and the vertical axis shows an index related to the strength of the substorm, both in arbitrary units. Three different phases of the storm are indicated: the growth phase, expansion phase and recovery phase. [6]

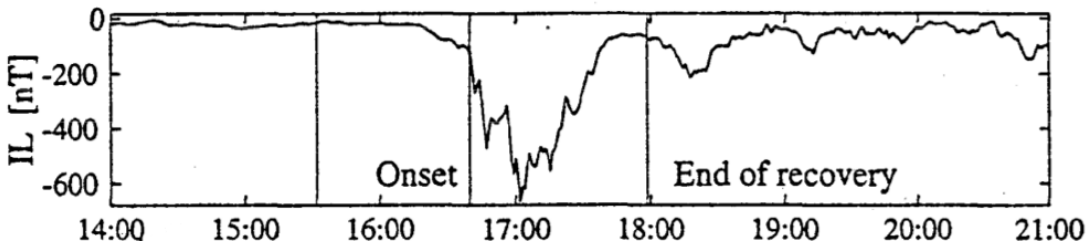

Figure 2: A plot showing the IL index (index used to describe the strength of a magnetic substorm) over time. The plot shows that the time scale of the event is a few hours. [7]

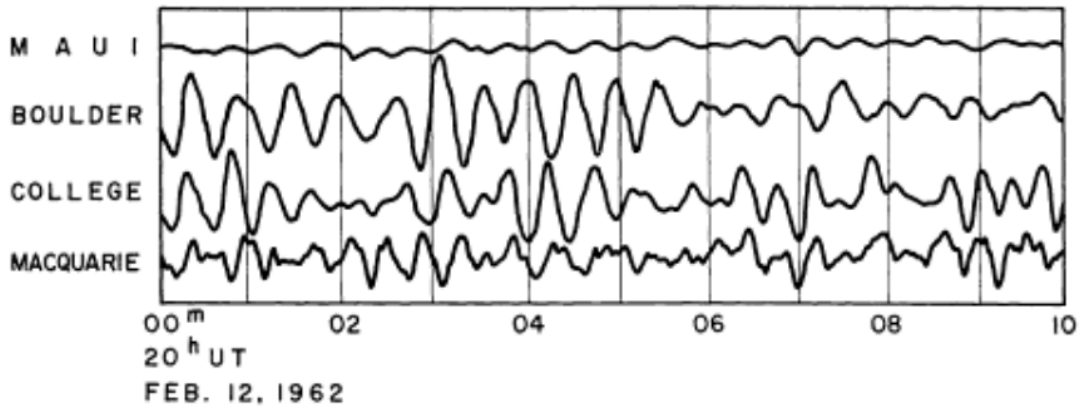

Figure 3: A record of the gmeomagnetic field strength over time, showing a pulsation event in the 0.02-0.1 hertz range (Pc3). The event occurred in 1962 and was recorded simultaneously at four stations. [8]

2.2 Models of the Earth's magnetic field

The Earth's magnetic field is an ever-changing vector field that is usually split into either two or three components. The two-component system comprises the horizontal component H, tangent to the surface of the Earth, and the vertical component Z, normal to the surface of the Earth. In addition to these components, a third coordinate is needed: deviation between the geographical and magnetic north poles, which is called declination D.

The components in the three-component system are the X component pointing to the geographic north, the Y component pointing east and the Z component, normal to the surface of the Earth. The X and Y components are tangential to the surface of the Earth. It is noteworthy that the Z component in both component systems is pointing down. Both component systems are visualized in Fig. 4.

2.2.1 Dipolar models

The most common model of the Earth's magnetic field is a simple dipole field, similar to a bar magnet. The idea that the Earth's magnetic field could be represented like that of a normal magnet originated in 1600 from William Gilbert's book "De Magnete", in which he stated "Magnus magnes ipse est globus terrestris" [9]. This Latin phrase can be freely translated as "The Earth itself is a great magnet". Using a magnetized iron sphere Gilbert could simulate the change in inclination as a function of latitude on the

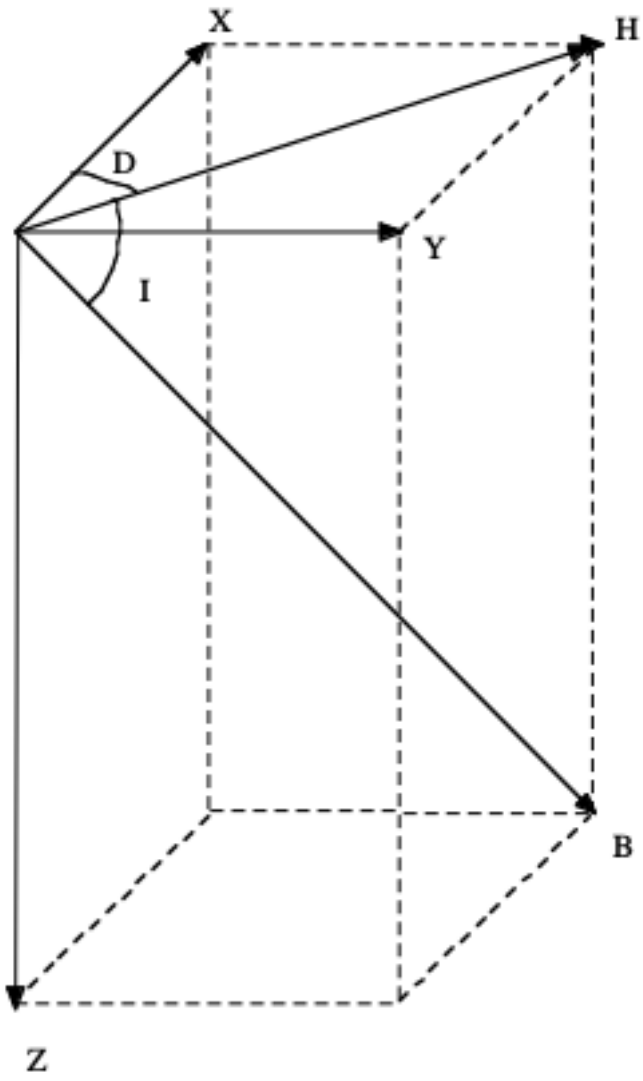

Figure 4: The two different component systems of the Earth's magnetic field. In the two-component system H is the total horizontal component, Z the vertical component and D the deviation between the geographic and magnetic north poles. In the three-component system X is the horizontal component pointing to the geographic north, Y the horizontal component pointing east and Z the vertical component. I is the angle between the total magnetic field vector B and the tangent of the Earth's surface. [4]

sphere, a phenomenon observed when using a compass for navigation. This indicated that the Earth's field was similar to the field of a spherical magnet.

The simplest of the dipolar models is an axial dipole, in which the dipole axis is parallel to the Earth's rotational axis [4]. This field is only dependent on the distance from the center of the Earth r and latitude ϕ:

$$H = \frac{\mu_0}{4\pi}\frac{m}{r^3}\cos\phi \tag{1}$$

$$Z = 2\frac{\mu_0}{4\pi}\frac{m}{r^3}\sin\phi \tag{2}$$

$$B = \frac{\mu_0}{4\pi}\frac{m}{r^3}\sqrt{4-3\cos^2\phi}, \tag{3}$$

where m is the magnetic dipole moment of the Earth and $\frac{\mu_0}{4\pi}$ is a qualitative constant equal to 10^{-7} Tm/A [4]. It should be noted that the axial dipole model does not account for declination: the magnetic poles are located at the geographical poles.

The axial dipole model can be improved by tilting the axial dipole by about 11 degrees. The equations of the magnetic fields themselves remain unchanged, but the geographical coordinates must be replaced by so called dipole coordinates Φ and Λ:

$$\Phi = \arcsin(\sin\phi_0\sin\phi + \sin\phi_0\cos\phi\sin(\lambda-\lambda_0)) \tag{4}$$

$$\Lambda = \arccos(\cos\phi\frac{\sin(\lambda-\lambda_0)}{\cos\Phi}), \tag{5}$$

where ϕ and λ are the geographical latitude and longitude, respectively, and ϕ_0 and λ_0 refer to the geographical location of the geomagnetic poles [10].

The tilted dipole field does not take into account the fact that the magnetic field is not symmetrical between the hemispheres. A better approximation can be achieved by moving a simple dipole model roughly 500 kilometers to the northern hemisphere [4]. The simples of such displace dipole fields is a radial dipole. The magnetic moment vector of a radial dipole field is always parallel to the Earth's radius and is located on the Earth's rotation axis at a distance of r_0 from the center of the Earth. The H and Z

components of such a field are

$$H = \frac{\mu_0}{4\pi}\frac{mQ}{R_e^3\rho_e^3}(1 + \frac{3q_0(P-q_0)}{\rho_e^2}) \tag{6}$$

$$Z = \frac{\mu_0}{4\pi}\frac{mQ}{R_e^3\rho_e^3}(\frac{3(P-q_0)(1-Pq_0)}{\rho_e^2} - P), \tag{7}$$

where

$$\rho_e = \sqrt{1 + q_0^2 - 2Pq_0} \tag{8}$$

$$q_0 = r_0/R_e;\ P = \delta\sin\phi;\ Q = \delta\cos\phi \tag{9}$$

and R_e is the radius of the Earth and ϕ and δ the geographical latitude and longitude.

2.2.2 Multipole models

The best representation of the Earth's magnetic field is the multipole model, which approximates the field as a sum of several multipolar fields [11]. The multipole model was proposed by Gauss in 1839. His proposed presentation was based on the fact that in an area with zero electrical current near the Earth's surface the magnetic field's curl and divergence are zero:

$$\nabla \times \mathbf{B} = 0 \tag{10}$$

$$\nabla \cdot \mathbf{B} = 0 \tag{11}$$

Since the field's curl is zero, the field has a scalar potential U so that

$$\mathbf{B} = -\nabla U \tag{12}$$

and from the divergence being zero follows that Laplace's equation can be applied to the potential:

$$\nabla^2 U = 0 \tag{13}$$

This means that U is harmonic and it can be solved in spherical coordinates using spherical harmonics. Using a spherical coordinate systems with coordinates (r, θ, ϕ) the equation can be presented as

$$\frac{1}{r}\frac{\partial^2(rV)}{\partial r^2} + \frac{1}{r^2\sin\theta}\frac{\partial}{\partial\theta}(\sin\theta\frac{\partial V}{\partial\theta}) + \frac{1}{r^2\sin^2\theta}\frac{\partial^2 V}{\partial\phi^2} = 0, \tag{14}$$

where r is the radius of the sphere, θ the polar angle and ϕ the longitude [12]. The solutions to this equation are of the form

$$\begin{aligned} V_{n,m}(r,\theta\phi) = a\sum_{n=1}^{\infty}\sum_{m=0}^{n}([A_{n,m}\cos m\phi + B_{n,m}\sin m\phi](\frac{a}{r})^{n+1} \\ +[C_{n,m}\cos m\phi + D_{n,m}\sin m\phi](\frac{r}{a})^{n})P_{n,m}(\cos\theta) \end{aligned} \tag{15}$$

where $P_{n,m}$ are associated Legendre functions. The Legendre functions are usually presented in the form

$$P_{n,m}(\mu) = (1-\mu^2)^{m/2}\frac{\mathrm{d}^m P_n(\mu)}{\mathrm{d}\mu^m}, \tag{16}$$

where $\mu = \cos\theta$ and $P_n(\mu)$ are the usual Legendre functions. $A_{n,m}, B_{n,m}C_{n,m}$ and $D_{n,m}$ are called spherical harmonic coefficients, n and m are the degree and the order of $P_{n,m}(\cos\theta)$, respectively and a is the radius of the Earth. The degree n denotes the degree of the multipole contributing to the field: for a dipole $n = 1$, for a quadrupole $n = 2$, for an octupole $n = 3$ and so on. Since magnetic monopoles have not been observed in nature, the minimum value for $n = 1$. Terms multiplied by $(\frac{a}{r})^{n+1}$ are related to the Earth's internal sources, since when r approaches infinity the terms go to zero, while terms multiplied by $(\frac{r}{a})^n$ describe sources originating outside the Earth, since these terms go to zero when r goes to zero. From Eq. 15 we can write the components of the magnetic field in the spherical coordinate system using Eqs. 12 and 14:

$$\begin{aligned} B_r = \frac{-\partial V}{\partial r} = \sum_{n=1}^{\infty}\sum_{m=0}^{n}((n+1)[g_n^m\cos m\phi + h_n^m\sin m\phi](\frac{a}{r})^{n+2} \\ - n[q_n^m\cos m\phi + s_n^m\sin m\phi](\frac{r}{a})^{n-1})P_n^m(\theta) \end{aligned} \tag{17}$$

$$\begin{aligned} B_\theta = \frac{-\partial V}{r\partial\theta} = \sum_{n=1}^{\infty}\sum_{m=0}^{n}([g_n^m\cos m\phi + h_n^m\sin m\phi](\frac{a}{r})^{n+2} \\ + [q_n^m\cos m\phi + s_n^m\sin m\phi](\frac{r}{a})^{n-1})\frac{\mathrm{d}P_n^m(\theta)}{\mathrm{d}\theta} \end{aligned} \tag{18}$$

$$\begin{aligned} B_\phi = \frac{-1}{r\sin\theta}\frac{-\partial V}{\partial\phi} = \frac{1}{sin\theta}\sum_{n=1}^{\infty}\sum_{m=0}^{n}([g_n^m\sin m\phi - h_n^m\cos m\phi](\frac{a}{r})^{n+2} \\ + [q_n^m\sin m\phi - s_n^m\cos m\phi](\frac{r}{a})^{n-1})\frac{\mathrm{d}P_n^m(\theta)}{\mathrm{d}\theta} \end{aligned} \tag{19}$$

Here g_n^m, h_n^m, q_n^m and s_n^m are spherical harmonic coefficients.

As stated previously, the magnetic potential contains terms describing both sources

inside the Earth and outside the Earth. The internal and external components of the magnetic field can be derived from the potential shown in Eq. 12 [4]:

$$
\begin{aligned}
B_{\theta_i} &= -\sum_{n=1}^{\infty}[(\frac{a}{r})^{n+2}\sum_{m=0}^{n}(g_n^m\cos m\phi + h_n^m\sin m\phi)\frac{\mathrm{d}P_n^m(\theta)}{\mathrm{d}\theta}] \\
B_{\phi} &= -\frac{1}{r\sin\theta}\sum_{n=1}^{\infty}[(\frac{a}{r})^{n+2}\sum_{m=0}^{n}(g_n^m\sin m\phi - h_n^m\cos m\phi)\frac{mP_n^m(\theta)}{\sin\theta}] \\
B_{r_i} &= -\sum_{n=1}^{\infty}[(n+1)(\frac{a}{r})^{n+2}\sum_{m=0}^{n}(g_n^m\sin m\phi + h_n^m\cos m\phi)P_n^m(\theta)]
\end{aligned}
\tag{20}
$$

$$
\begin{aligned}
B_{\theta_e} &= -\sum_{n=1}^{\infty}[(\frac{a}{r})^{1-n}\sum_{m=0}^{n}(q_n^m\cos m\phi + s_n^m\sin m\phi)\frac{\mathrm{d}P_n^m(\theta)}{\mathrm{d}\theta}] \\
B_{\phi} &= -\frac{1}{r\sin\theta}\sum_{n=1}^{\infty}[(\frac{a}{r})^{1-n}\sum_{m=0}^{n}(q_n^m\sin m\phi - s_n^m\cos m\phi)\frac{mP_n^m(\theta)}{\sin\theta}] \\
B_{r_i} &= -\sum_{n=1}^{\infty}[n(\frac{a}{r})^{1-n}\sum_{m=0}^{n}(q_n^m\sin m\phi + s_n^m\cos m\phi)P_n^m(\theta)]
\end{aligned}
\tag{21}
$$

The subscripts in these equations denote internal (i) and external (e) sources of magnetic field. The components described in Eqs. 20 and 21 are conveniently identical to components in a 3-dimensional Cartesian coordinate system. The B_θ component corresponds to a northward component (usually denoted by X), B_ϕ corresponds to an eastward component (Y) and B_r to a component normal to the Earth's surface (Z). This makes Eqs. 20 and 21 easy to use when modeling the magnetic field of the Earth and comparing the calculated models to measurements.

2.3 History of magnetometers

Interest in the study of the Earth's magnetic field started in China around 200 BC with the invention of the compass [1], [13]. The first compass was a spoon-shaped piece of lodestone, a magnetic ore, that was probably used for finding gemstones and selecting suitable places for houses. Later on, before 1000 AD, the Chinese developed suspended needle compasses, which comprised a magnetized needle suspended from a silk thread. By 1200 AD in Europe it was supposed that the compass aligned itself with the pole star, since unlike other stars, the pole star would not move in the sky.

The first magnetometer that saw widespread use was built by Carl Friedrich Gauss

in 1832 [14]. The magnetometer consisted of a permanent magnet suspended on a gold wire. Gauss would deflect the magnet and record the time period of its oscillations. Using this method he measured the intensity of the field. Previous measurements only considered the direction of the field, since most magnetic measurements were done for navigational purposes. Gauss was the first to design an instrument for measuring the intensity of the field. Devices based on this same principle - suspending a permanent magnet on a wire and recording its movement - were used well into the 20th century [15]. They fell out of use during the later years due to their reliance on delicate mechanism and needing lots of maintenance.

William Thomson, better known as Lord Kelvin and famous for his studies on thermodynamics, discovered the magnetoresistive effect in 1856 [16]. This effect states that the electrical conductivity of some materials changes as a function of ambient magnetic field. Thomson studied this effect on iron and nickel, and later on other researchers expanded his results. New types of magnetoresistance were discovered, including for example giant magnetoresistance (GMR) in 1988 [17].

A new effect that formed the basis for a new generation of magnetometers was discovered by Edwin Hall in 1879 [18]. The Hall effect is an effect observed in current-carrying conductors, where a measurable voltage forms in a direction perpendicular to the direction of the current if an ambient magnetic field is present. This effect is widely used, even today, in small scale magnetometers such as those used in smartphones and other portable devices, much like GMR.

In 1936 Aschenbrenner and Goubau developed a new type of magnetometer, called the fluxgate magnetometer. It was originally used for detecting submarines in the World War II and later on in geomagnetic survey [19]. For example, measurements done using a fluxgate magnetometer confirmed the plate tectonic theory. Nowadays several manufacturers produce fluxgate magnetometers. They are suitable for scientific studies due to their high resolution (in the order of 0.01 nanoteslas), good linearity and temperature stability. Sensors manufactured in a certain configuration also show low noise levels, in the order of 0.01 nanoteslas [20]. They are also suitable for use in space due to their previously mentioned qualities and due to the fact that they are relatively easy to scale down in size.

2.4 History of geomagnetic measurements in the Arctic regions

One of the oldest, if not the oldest, time series of the geomagnetic field has been produced in Russia. The earliest single measurements of declination of the field were performed in the eighteenth century, and regular and continuous measurements were started in 1724 [21]. In 1829, the first observatory was established in St. Petersburg [22]. The Russian Hydrometeorological Service, Roshydromet, was started in 1921 and has since started new measuring stations around the Arctic region and produced a continuous timeseries from several stations around Russia. [23]

Finland has a long history in the study of geomagnetism. The first geomagnetic observatory was established by Johan Jakob Nervander in Helsinki in 1838 by an order from the Russian emperor Nicholas I. The observatory building was finished in 1841 in Kaisaniemi and observations began in 1844. The instruments were state of the art of the time and the operators were highly trained to perform the best possible measurements. The produced timeseries is of very high quality and is still used in research. Magnetic observations were stopped in 1912 due to electric tramways producing too much interference in the measurements. Later on, the observatory developed into the modern Finnish Meteorological Institute. [24]

Finnish geomagnetic measurements were stopped for a few years due to the shutting down of the observatory in Kaisaniemi. In 1914, the Sodankylä Geophysical Observatory started operation and has since produced an almost unbroken timeseries, only briefly stopping because of the war in Lapland in 1944, but restarted in 1947 and continuing unbroken ever since. Later on, another observatory was established in Nurmijärvi in Southern Finland [25]. The measurements in Nurmijärvi started in 1950s and have continued to this day [26].

Finnish observatories and measurement stations are part of international measurement networks, largest of which are Intermagnet and IMAGE. Intermagnet includes the Nurmijärvi and Sodankylä observatories, while IMAGE also includes the unmanned stations in Kevo, Kilpisjärvi, Muonio, Sodankylä, Pello, Ranua, Oulujärvi, Mekrijärvi and Hankasalmi. [27], [28], [Tanskanen 2009]

3 Types of magnetometers

Magnetometers can be divided into a few different categories. One is based on the type of their signal: analog or digital. Another is the type of measurement they're capable of: vector magnetometers, which measure one or more components of the vector field, recording the strength and direction of the field, or absolute magnetometers, which record only the strength of the field.

3.1 Analog magnetometers

Analog magnetometers are instruments that perform measurements and store information in an analog format. All classical magnetometers are analog magnetometers. Analog magnetometers fell out of use and were replaced by digital instruments due to the latter requiring less maintenance, having better automatization possibilities and larger data storage capabilities.

The era of widespread magnetometric measurement campaigns begun when the British Navy started mapping the direction of the Earth's magnetic field using Gauss magnetometers equipped with cameras to automatically record the movement of the sensor [29]. Before this, all measurements had to be recorded by hand. Automatic measurements drastically reduced the manpower needed and thus opened new possibilities in assaying the magnetic field.

3.1.1 Gough-Reitzel

One example of an analog magnetometer is the Gough-Reitzel magnetometer. It is a classical magnetometer, similar to one built by Gauss, but it was capable of measuring the complete vector field: the vertical component Z, horizontal component H and declination D. The instrument consisted of three permanent magnets, one for each component, equipped with small mirrors. A light source provided three beams of light, which in turn were reflected to a photographic film by the mirrors on the magnets. Changes in the geomagnetic field deflected the magnets and the mirrors, moving the light beams on the photographic film and thus recording the changes in the field. Fig. 5 shows a Gough-Reitzel magnetometer and a more detailed view of one of the sensors, with the wire supporting a permanent magnet and a mirror.[30]

The Gough-Reitzel magnetometers were very accurate and had a high resolution of

(a) The magnetometer is roughly 1.5 meters tall. The rectangular piece on the top is the light source and camera.

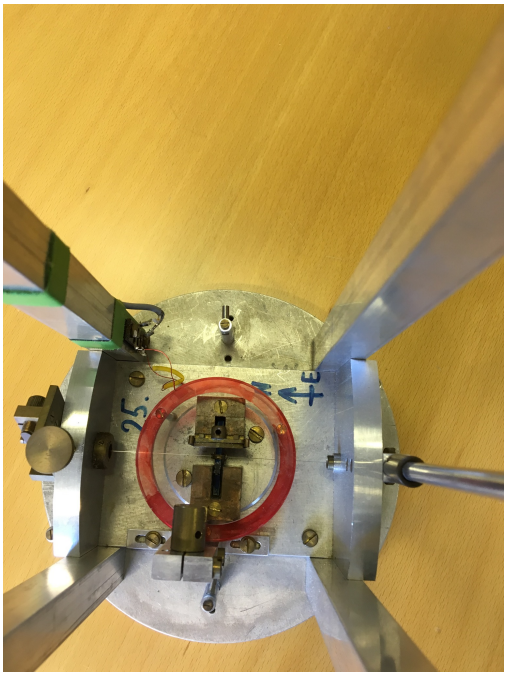

(b) The metal wire holding the magnet runs horizontally in the picture. The red circle is a coil used to calibrate the magnetometer.

Figure 5: An overview image of a Gough-Reitzel magnetometer (a) and a close-up (b) of one of the three sensors.

0.1 nanoteslas and they were capable of performing measurements independently for two months. A downside of these instruments was that they were precise, mechanical devices. They were prone to jamming and required careful calibration before use. Being mechanical, they were very sensitive to vibration. To mitigate this, they were buried deep underground. Also, the photography film was a finicky medium for storing data. The film would sometimes get jammed or overexposed, causing data to be lost. Recovery of the data produced by some Gough-Reitzel magnetometers is discussed in more detail in section 4.

3.2 Digital magnetometers

Digital magnetometers started replacing analog instruments when digital technology developed to the point of being affordable. Digital instruments have several advantages over analog ones: data storage is easier, safer and more compact, power consumption can be lowered to a fraction of analog instruments and with proper infrastructure, completely

independent operation can be achieved. The basic operating principle behind digital instruments is to generate some kind of a voltage signal and then record it in a digital format. Many of the sensors used in these instruments can be used in analog applications too, but then all the advantages of digitalization will be lost.

3.3 Fluxgate magnetometers

Fluxgate magnetometers are the most widely used sensor type in geomagnetic measurements. They are vector magnetometers, usually consisting of three sensors in an orthogonal arrangment, each of which measures one component of the geomagnetic field. Fluxgate magnetometers consist of two coils and a ferromagnetic core. An alternating current is driven through one of the coils. The current produces an alternating magnetic field in the core and the other coil is used to sense the field in the core. If an external field is present and it is parallel to the core, it will produce an observable offset in the strength of the magnetic field in the core. Fig. 6 shows a typical fluxgate sensor configuration and response to a changing external magnetic field. The sensor can only sense magnetic fields parallel to the core. An alternative configuration, where the ferromagnetic core is shaped like a ring, produces lower noise levels [31]. Fluxgate magnetometers are very versatile and their uses range from handheld devices to observatory magnetometers to satellite instruments. They are easy to use and when manufactured to high standards produce excellent data.

3.4 Magnetoresistive sensors

Magnetoresistive sensors can use one of several different types of magnetoresistivity. For sensing the direction of a magnetic field, eg. anisotropic magnetoresistivity (AMR) can be used. In anisotropic magnetoresistivity, the resistivity of a material changes as a function of the angle between its magnetization and electrical current traveling through the material due to conduction electron scattering off of the magnetic momenta of impurity atoms in the material. The resisitivity due to anisotropic magnetoresistance is

$$\rho(\xi) = \rho_{\perp} \sin^2(\xi) + \rho_{\parallel} \cos^2(\xi), \tag{22}$$

where ξ is the angle between the current and the magnetization, $\rho_{\perp}$ is the resisitivity in the direction perpendicular to the current and $\rho_{\parallel}$ is the resisitivity in the direction parallel to the current [33]. The exact mechanism of the change in resistivity depends on the material and a more detailed description is outside the scope of this thesis. For example, the HMC5883L and HMC2003 manufactured by Honeywell utilize the

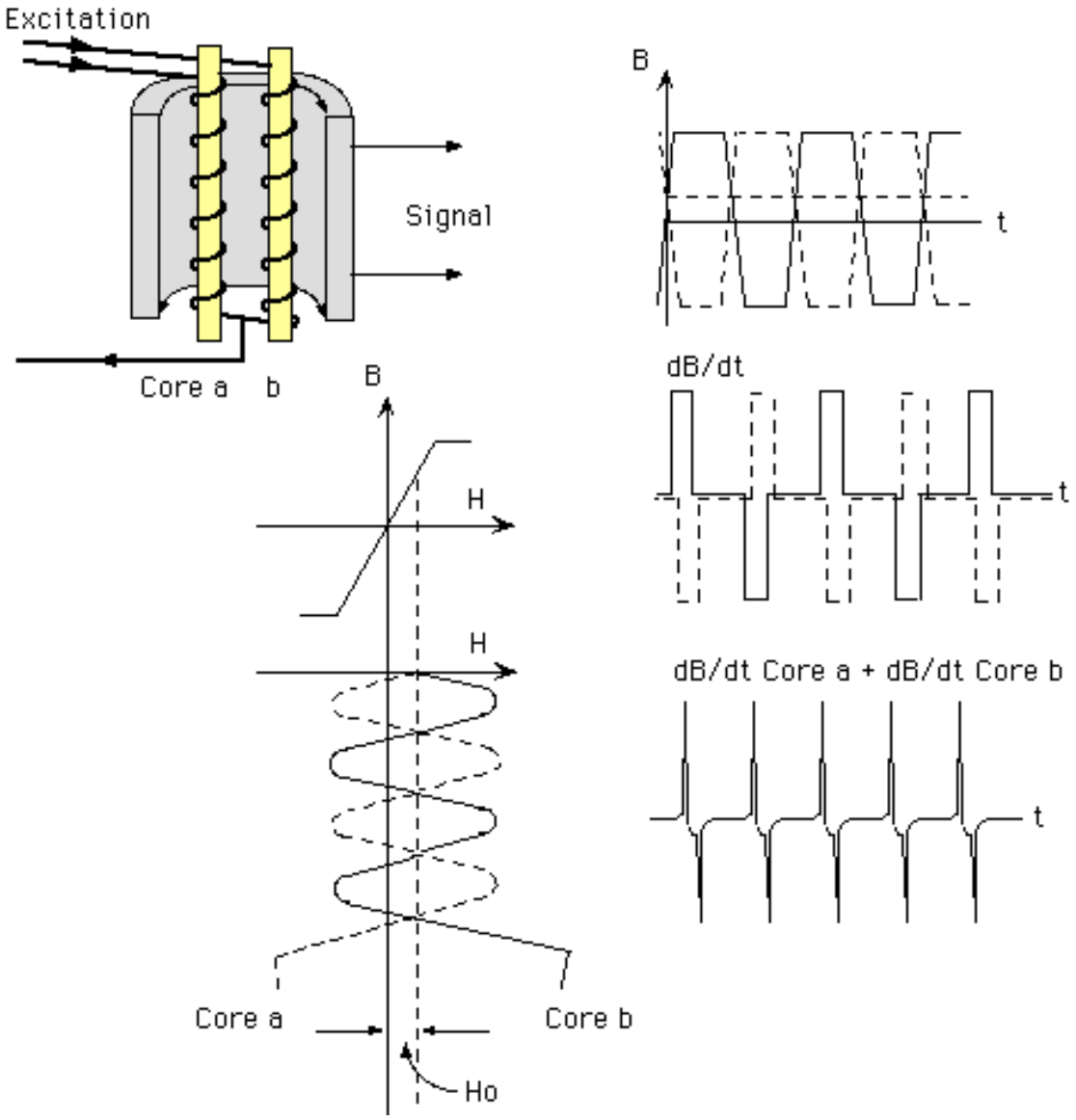

Figure 6: A fluxgate magnetic sensor with a bar core configuration, qualitatively showing the signal produced by a fluxgate magnetometer. [32]

magnetoresistive effect to measure magnetic fields. The use of HMC2003 in a scientific quality instrument is described in more detail in sections 5 and 7.

3.5 Hall effect sensor

Hall effect sensors are often used in teaching laboratories due to their simple mechanism. They can also easily be miniaturized, allowing their use in applications where space is a limited resource. Hall effect sensors are direction-dependent, making them suitable for use in vector magnetometers.

If a current is placed in an external magnetic field, the charge carriers start drifting from their original direction due to the Lorentz force caused by the magnetic field. Only the component of the field that is perpendicular to the direction of the current applies a force:

$$\mathbf{F} = q(\mathbf{E} + (\mathbf{v} \times \mathbf{B})), \tag{23}$$

Where (F) is the Lorentz force, $\mathbf{E}$ is the electric field permeating the system including the field of the charge carriers themselves, $\mathbf{v}$ is the drift velocity of the charge carriers and $\mathbf{B}$ is the external field. Charge carriers of different polarities drift to the opposite sides, creating a voltage perpendicular to the direction of the current. This voltage is directly proportional to the external field:

$$V_{\mathrm{H}} = \frac{I_x B_z}{nte}, \tag{24}$$

where V_{H} is the Hall voltage, I_x is the current through the conductor, B_z the perpendicular component of the external field, n is the charge carrier number density, t is the conductor's thickness and e is the elementary charge.

Hall effect sensors are not often used in geomagnetic measurements due to the low signal levels. Since the strength of the geomagnetic field is of the order of 10 000 nanoteslas, the operating current would have to be rather high to produce noticeable voltages, or the signal would have to be amplified with a very low noise amplifier.

3.6 Absolute magnetometers

Absolute magnetometers measure only the absolute strength of the magnetic field, so they are direction-independent. One of the most widely used absolute magnetometers is a so-called proton-precession magnetometer. The magnetometer measures the voltage

induced in a pick-up coil by the precession of protons in a hydrogen-rich fluid, like gasoline or water.

First, the liquid in the sensor is subjected to a strong external magnetic field, usually produced with a solenoid and direct current. This orients the proton's magnetic moments in one direction. After orienting the protons, the external field is shut off. This causes the protons to return to a relaxed state and precess with an angular frequency

$$\omega = \gamma B, \tag{25}$$

where γ is the gyromagnetic constant and B is the strength of the field being measured. This is known as the Larmor equation. Since the protons precess, they release their excess energy through radiation. The frequency of this radiation is directly related to the external magnetic field and thus the strength of the field can be determined.

More precise measurements can be obtained using a magnetometer based on the Overhauser effect. Instead of polarizing the protons in a liquid with a DC field, some free radicals are introduced to the liquid. The spins of electrons of these free radicals are polarized using a radio-frequency field. The electron spins then couple to the protons in the liquid, which then release excess energy through precession. The relation between the external field and the precession frequency is the same as in eq. 25. The production of the RF field takes much less energy than that of a DC field. Also, the radio frequencies are well out of the band of the Larmour frequency and thus do not contribute any noise to the system.

4 Scandinavian magnetometer array

For the International Magnetoshperic Study (IMS) (1976-1979), a two-dimensional magnetometer array of unprecedented density was established in Scandinavia. The array was known as the Scandinavian Magnetometer Array (SMA) and it consisted of 36 Gough-Reitzel type magnetometers. The aim of the SMA was to study the time-dependent two-dimensional structure of substorm related magnetic fields at the surface of the Earth. The magnetometers were built to the highest standards available at the time and were capable of two months of independent operation at a time, after which their storage media were full and their batteries depleted. [34]

Some stations started operation as early as 1974, before IMS, and some continued operation until 1981. The downside of the magnetometers was the chosen storage medium: the data was saved on reels of photosensitive film, preventing automatic digitization and thus comprehensive statistical analysis of the data. Each reel contains roughly three months of measurements and the campaign produced over 600 reels, so a lot of data of excellent quality has gone largely unused due to the fact that the data has to be digitized manually. Some key events have been digitized and thus some analysis has been done, but the full time series has never been analyzed, even though there is demand for the full digitized time series. [35], [36]

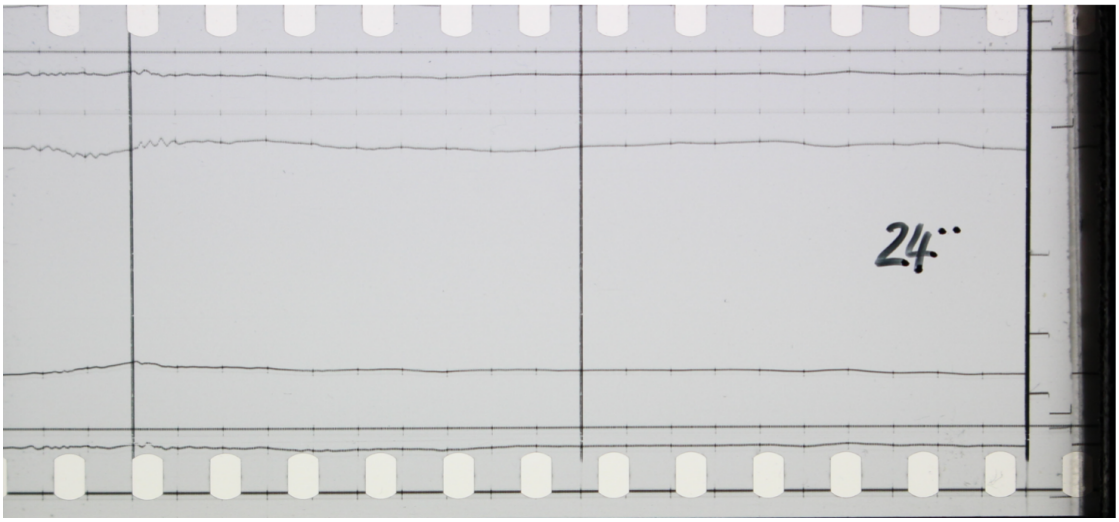

Figure 7: An example of the scanned SMA films. This example shows one of the problems: handwritten timestamps on the films, left over from when the data was searched through for notable events.

In my thesis work, I developed an automatic digitization method for the SMA data using Matlab. First step in the process was scanning the films into a digital format. Some commercial devices are available, but better results were achieved with a custom built scanner which consisted of a mechanism which moved the film one frame a time and triggered a digital camera which took a photo of the film. An example of the result of such a scan is shown in Fig. 7.

After scanning the films, the values represented by the plots on the film needed to be read from the film. Each reel has a datasheet in the beginning, telling the scale on the film as nanoteslas per millimeter in the vertical direction. Time resolution was also

written on the datasheets. The scanning process was as follows:

1. Crop the picture, cutting out the holes of the film and the black bar on the right
2. Look for black spots in the leftmost column. The vertical locations of these spots are the rough locations of each of the plots.
3. Move to the next column and search for a new black spot around the location of the black spot in the previous column.
4. Repeat step 3 until the picture has been scanned.

As an example, the data scanned from Fig. 7 is shown in Fig. 8. As can be seen, the process can easily identify even rather small scale features of the data, eg. the small ripples in the upper left corner.

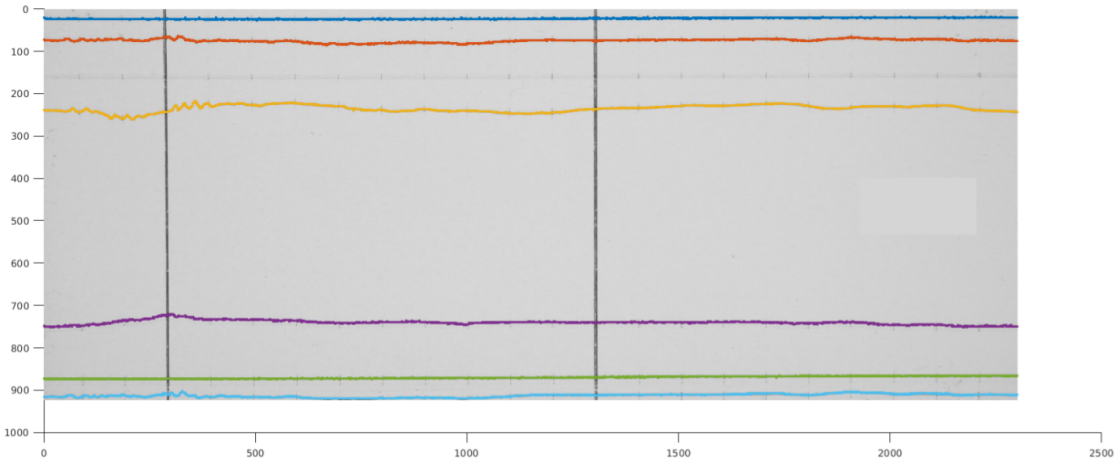

Figure 8: Results of the scanning process of the data in Fig. 7. Note the missing timestamp on the righthand side.

Despite the promising results, the scanning process is still challenging. Fig. 7 shows one example of these hindrances: handwritten timestamps. Luckily, it is possible and straightforward to identify and remove these stamps using Matlab's built-in computer vision toolbox.

Some other features of the data cause more problems. First, some of the data is over-exposed (for example in Fig. 9) and thus there are large dark areas covering the plots, making it extremely difficult to read them. Another problem is the structure of the plots themselves: they are not actually continuous lines, but consist of small black spots, as

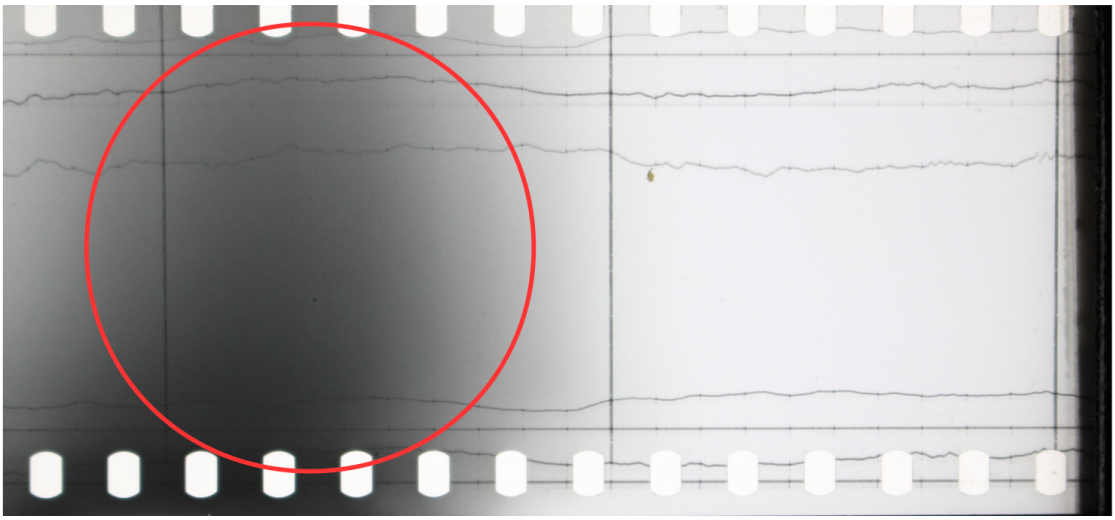

Figure 9: An overexposed region in the data. The algorithm cannot discern between a real data point and a generally dark background.

shown in Fig. 10. During strong changes of magnetic fields, these spots become separated from each other which makes it difficult for the process to follow them. These challenges are still unsolved.

Despite being very high quality and offering a unique view of the 2-dimensional structure of the geomagnetic field near the North pole, the analog nature of the data is problematic. High cost of state-of-the-art magnetometers prohibits arranging similar campaigns in the modern times. Thus, to possibly allow a similar campaign in the future, it is necessary to develop more affordable and accessible instruments.

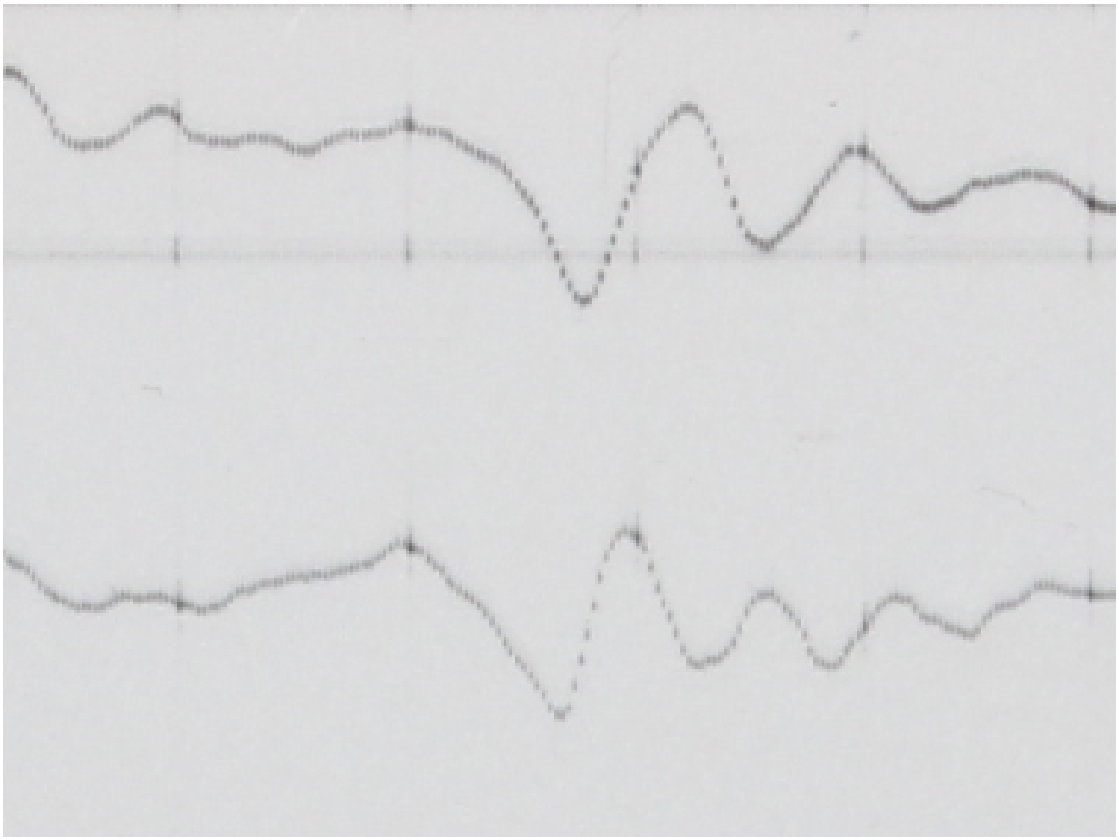

Figure 10: Separation of data points. Since the algorithm searches for a black spot from every column, it can't follow the plot if the data points are separated as in this picture.

5 Low-cost autonomous measurement stations

Advancements in production methods, materials and integrated circuit designs has made completely autonomous measurement stations a viable option for measurement campaigns. Low-cost computers, like the Raspberry Pi, that can run full-size operating systems, e.g. Debian Linux, combined with cheap sensors make setting up stations easy and affordable [37], [38]. Most low-cost computers and sensors are also often small in physical size, so the placement of the instruments is rather easy. A Raspberry Pi 2 combined with a small IC vector magnetometer costs around 400 euros including enclosure, power supply and data storage and achieves a resolution of fractions of microteslas [39]. The lower price comes also with a downside: instruments built in a scientific institute such as the LEMI-025 at Lviv Center of Institute for Space Research in Ukraine or the SFGE at the Technical University of Denmark cost thousands of euros, but achieve

thousands or tens of thousands times higher resolution in the order of 0.1 nanotesla or better [20], [40]. Of course, modern magnetometer stations require some infrastructure: a power supply and data connection are required so the magnetometer can run without the need for an operator to visit the station to retrieve data and change batteries every now and then.

5.1 Hardware

An autonomous magnetometer station requires a sensor and a controlling unit. Depending on the choice of sensor, an external ADC may be needed to achieve a reasonable resolution. The controlling unit can be any microcontroller or small computer capable of reading the sensor and sending or saving the data for further analysis.

5.2 MET magnetometer station

Metsähovi Radio Observatory in Kirkkonummi, Finland was chosen as the location for a Raspberry Pi based magnetometer due to the availability of a steady power supply and network connection. With minimal work, the magnetometer received power and was connected to the Internet via the local network of the observatory.

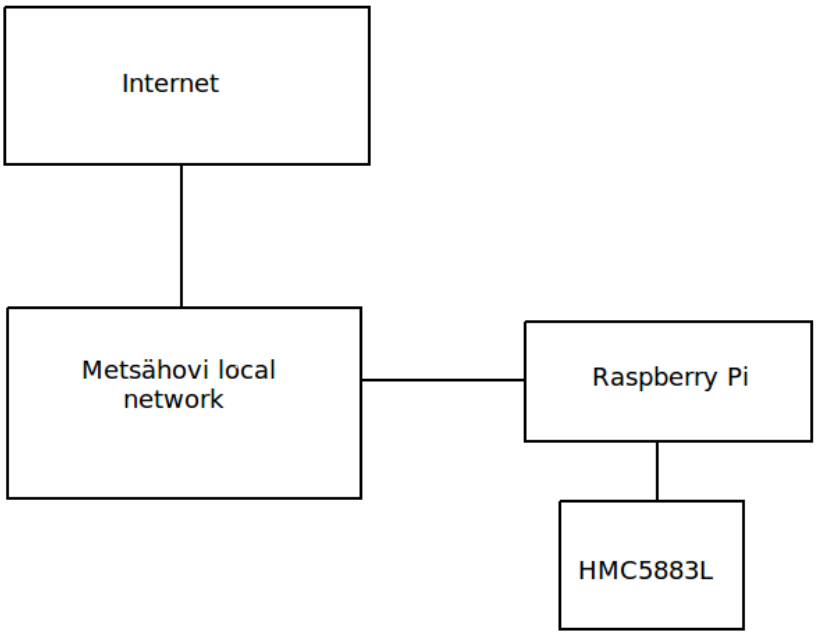

Figure 11: A block diagram of the Metsähovi magnetometer. The HMC5883L is connected to the Raspberry Pi over I2C, the RPi to the Metsähovi local network over Ethernet and the Metsähovi network to the internet. The RPi could be accessed by SSH'ing to the Metsähovi network and then SSH'ing to the RPi.

5.2.1 Controller

The Raspberry Pi 2 miniature computer was chosen as the controller for the Metsähovi magnetometer station. Several factors influenced the choice, including low cost, included hardware and connectors, physical size and ease of software development. Another viable candidate was the Arduino Uno R3 microcontroller, but the lack of network hardware on the Arduino ruled it out.

Raspberry Pi is a very widely used miniature computer (12.5 million units sold [41]) and thus, having a large userbase, has very extensive support. It has built-in general-purpose input-output (GPIO) connectors, allowing all kinds of peripherals to be used with the computer.

The Raspberry Pi, or RPi for short, is a miniature ARM-based computer capable of running a full operating system, for example Debian Linux. A Linux distribution called Raspbian, which is optimized for the RPi was installed on an SD card which functioned as the hard drive for the RPi.

The RPi is equipped with Ethernet, general purpose input and output (GPIO), USB, HDMI and audio connectors and can thus be used like a normal computer. The RPi requires a 5 volt and at least 1 ampere power supply. The GPIO connector can be used to extend the capabilities of the RPi by for example connecting different sensors, buttons and other devices. Some of the GPIO connectors also share pins with a built-in I2C chip and can be used to transmit data over the I2C protocol. In the case of the Metsähovi magnetometer, a Honeywell HMC5883L magnetometer was connected to the I2C bus. The RPi in it's enclosure is shown in Fig. 12.

5.2.2 Sensor

The HMC5883L is a 3D vector magnetoresistance based magnetometer manufactured by Honeywell. The magnetometer has a configurable dynamic range from ± 100 000 nanotesla to ±800 000 nanotesla and can achieve a resolution of 20 microgauss or 0.2 microtesla. The chip has a configurable gain and a built-in 12-bit analog-to-digital converter that saves the measurements for each axis in two 8-bit registers. Communication between the controller and the sensor is done over the I2C protocol. [39] At a supply voltage of 2.5 volts and a current draw of 100 μA the sensor requires very little power, so it can be powered by the Raspberry Pi. The sensor can be seen in with the RPi in Fig. 12 and a close up is shown in Fig. 13.

The HMC5883L can be configured using three 8-bit registers. The first register sets samples to be averaged, data output rate and possible positive or negative bias over the magnetoresistive sensor. The second register sets configurable gain and the third one sets the operational mode.

The HMC5883L has three different operational modes: continuous measurement, single-measurement and idle mode. In the continuous mode, the sensor makes a measurement and writes it in the output registers at up to 160 Hz. A new measurement is written to the register even if the controller has not read the previous value. In single mode, the

magnetometer waits for the controller to send a measurement command and writes the measurement to the output registers. After writing, the IC goes to idle mode and waits for a new measurement command.

The HMC5883L has been used in multiple satellite missions and was thus deemed appropriate for the Metsähovi magnetometer project [42, 43]. Also the low price and ready availability of the sensor played a role in the selection.

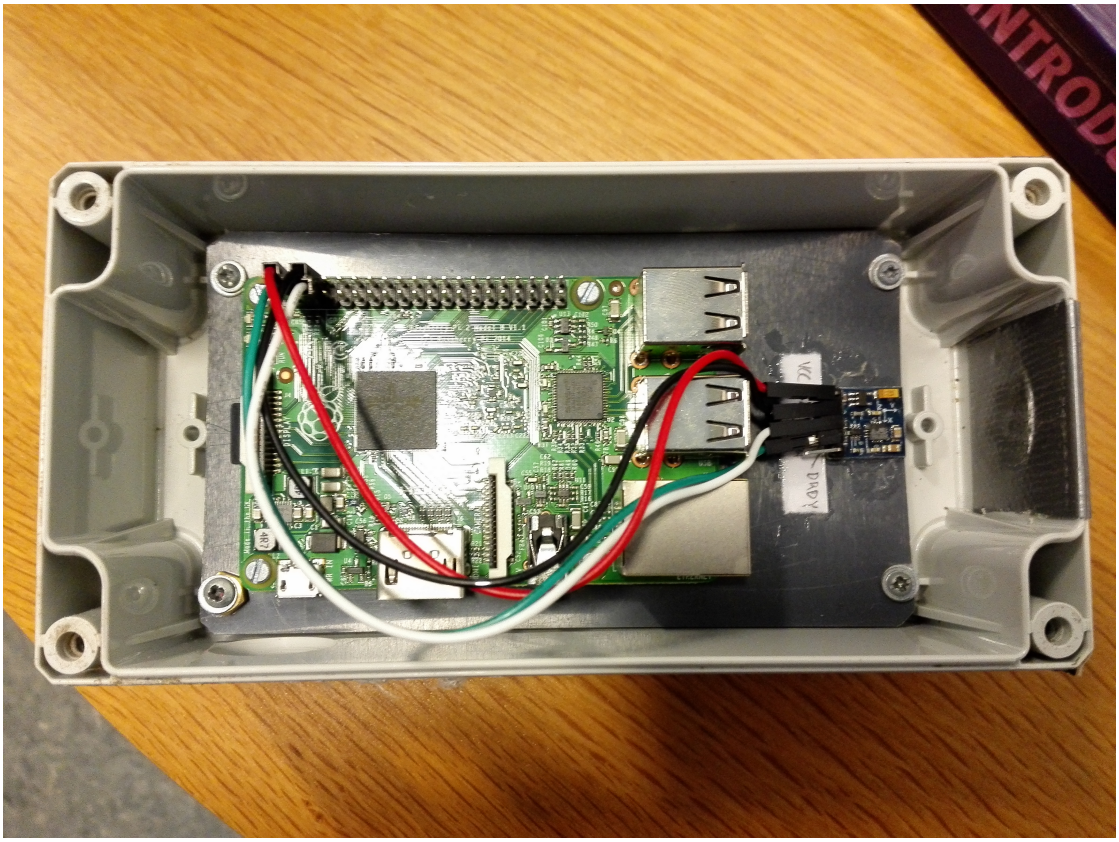

Figure 12: Picture of the insides of the magnetometer enclosure. The green circuit board is the Raspberry Pi and the smaller, blue board is the sensor. The grey base plate was used as an adapter between the screw holes in the Raspberry Pi and the enclosure.

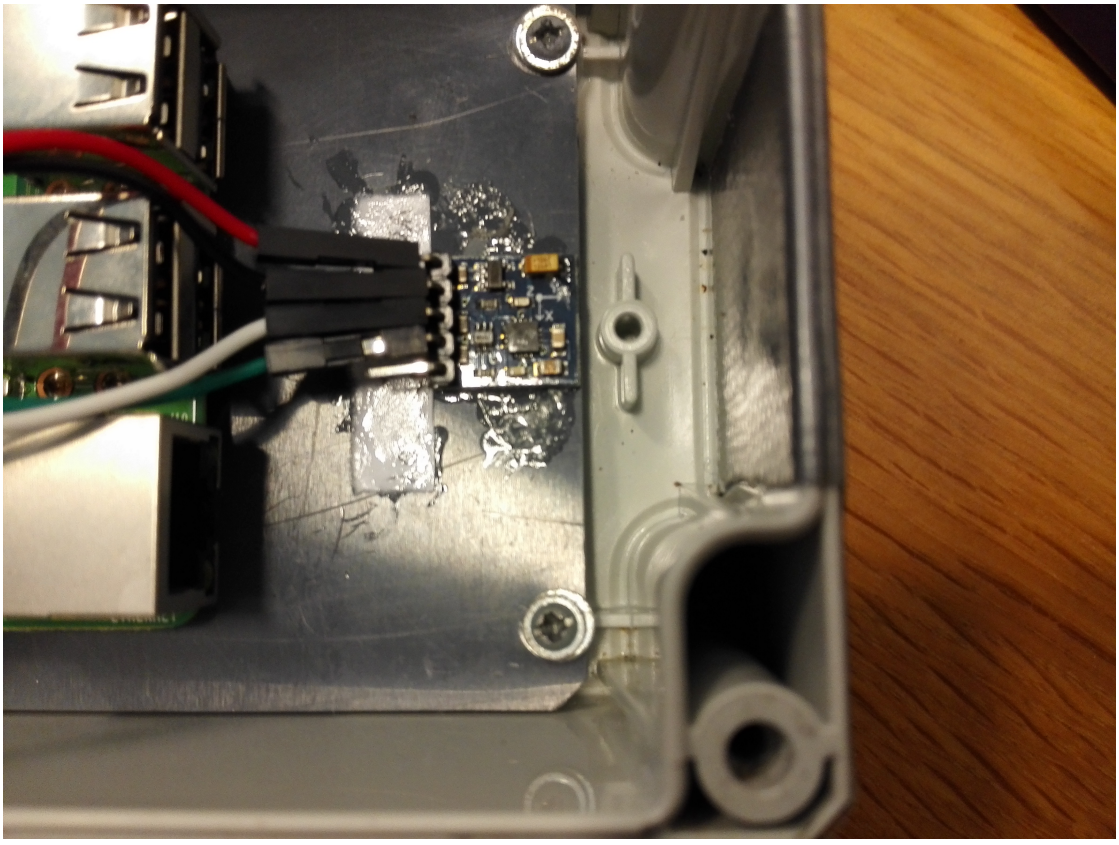

Figure 13: A detailed picture of the sensor. Due to the preliminary test nature of the instrument, the sensor was glued in place with no intention of replacing it on the same base plate.

5.3 Software

Since the RPi was running Linux, standard Linux tools were mostly available. The RPi was running a secure shell (SSH) daemon, allowing remote access to reconfigure and maintain the magnetometer remotely. Python was used to automate the measurements. A ready-made I2C Python module provided a connection interface to the sensor.

To keep costs down, free open-source tools were preferred. The Raspberry Pi can run Python, which has a plethora of ready-made libraries and thus is an easy language to work with. Unfortunately, Python is slow compared to compiled languages, requiring lots of resources to run sufficiently fast and reliably. Some potential issues include inaccuracies in measurement timestamps, but the low measuring frequency mitigates this problem.

Every day at 00:00 the RPi created a new text file on the SD card for the day's data. The RPi read the measurements from the HMC5883L at a frequency of 1 Hz and saved the results in the text file. At the end of each day, the RPi sent the data file to a predetermined list of recipients via e-mail.

To allow maintenance, the Python script was left running in a virtual terminal in the background. At login, the Raspberry Pi started a screen session or returned to an old session if one was found. In this virtual terminal, the operator could start the measurement script or move the virtual terminal to the background and perform maintenance on other parts of the system.

5.4 Results from Metsähovi

The Metsähovi magnetometer was operational for a total of 71 days from 22.8.2016 to 31.10.2016. Fortunately, the very next day a strong geomagnetic storm occurred and offered the perfect opportunity to test the magnetometer. The data from 23.8. are presented in Fig. 14. The geomagnetic field measured at the Nurmijärvi geophysical observatory is shown in Fig. 15. At around 8-9 in the morning the magnitude of the Y component starts dropping, indicating the onset of the storm. At around noon the magnitude of the Y component starts increasing again. In Fig. 14, the magnitude of each component is shown starting from 16.00. The strongest change is in the Y component, which decreases for the whole duration of the timeseries, while the Y component magnitude at Nurmijärvi is increasing during this time. The instrument was oriented differently at Metsähovi and the mismatch in gradient sign will be corrected after calibration. The fine features of the disturbance are lost, but nonetheless the magnetometer can be said to have detected the storm. This shows that the magnetometer can pick up very strong disturbances and is not affected by the large satellite dish of the observatory. The magnetometer was not calibrated before installation and thus the units in Fig. 14 are arbitrary.

The measurement campaign was originally intended to last longer than the 71 days, preferably over winter to make sure that the magnetometer could survive in the harsh conditions of Finnish winter. Unfortunately the SD card used as the data storage medium started degrading and by the 71 day mark, it was too corrupted to be able to reliably store data. Data points were missing, or incorrectly aligned with their timestamps which

made automated analysis if not impossible, very difficult.

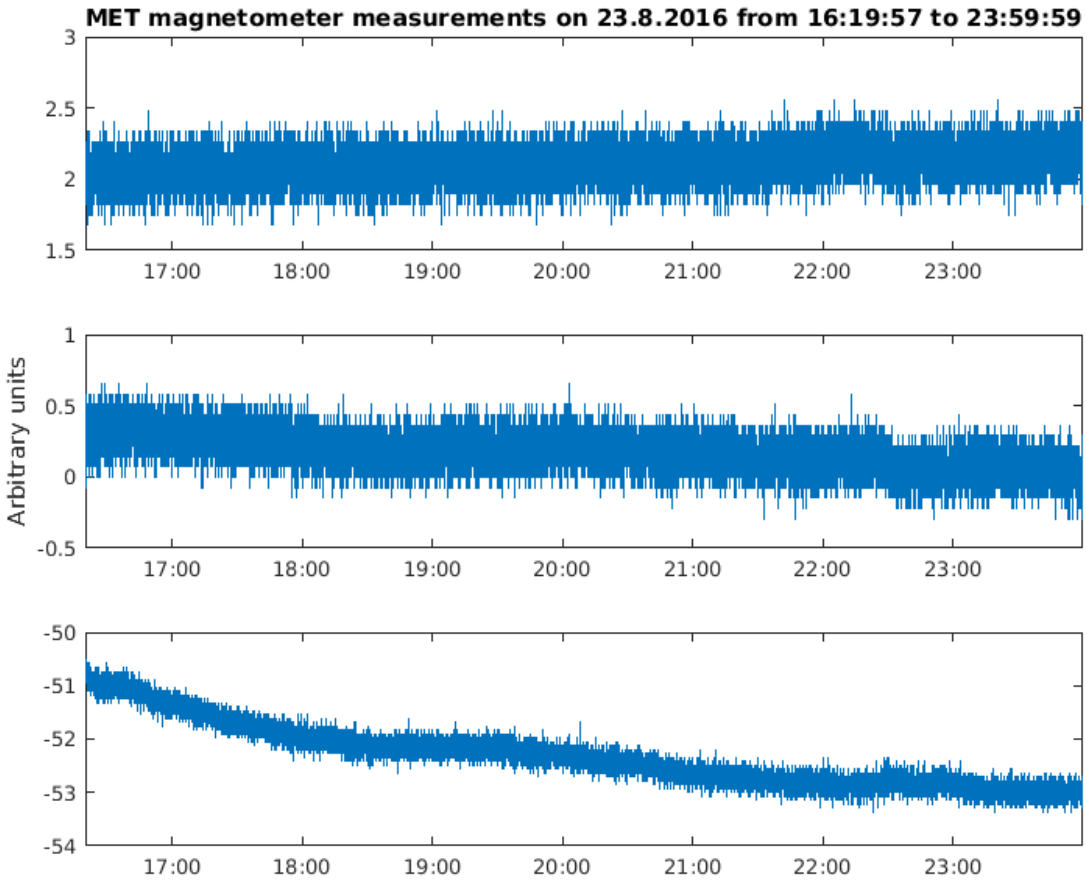

Figure 14: Data from the Metsähovi magnetometer. The top graph is the X component of the field, middle Z component and bottom Y component. The arbitrary units show the low resolution of the magnetometer, but despite that some variation of the magnetic field due to the storm is visible especially in the Y component.

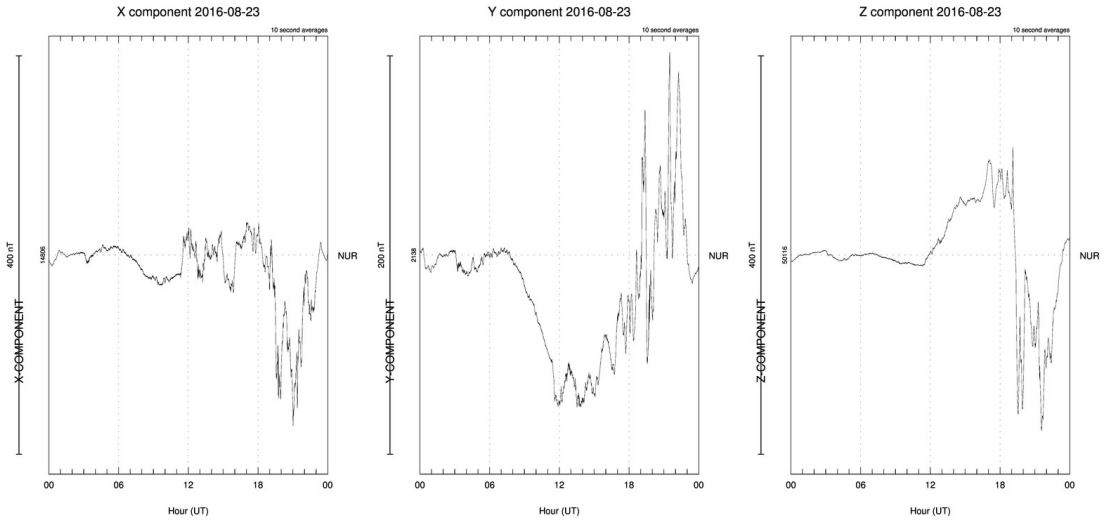

Figure 15: Geomagnetic data from the Nurmijärvi geophysical observatory. The plot shows all components of the geomagnetic field on 23.8.2016. A strong disturbance is clearly visible. Figure retrieved using the tool at `http://space.fmi.fi/image/www/index.php?page=user_defined`

Figure 16: Picture of the magnetometer in its enclosure. The hole on the side was used for passing power and data cables.

5.5 Improvements of the Metsähovi magnetometer

In 2017, the Metsähovi magnetometer station development continued. The HMC5883L sensor was replaced with three analog flux-gate sensors. The new sensor, FLC-100, has

a much higher sensitivity (order of 5 nanoteslas as opposed to the 0.2 microteslas of the previous HMC5883L) and a higher bandwidth [44]. The power consumption is higher, but that is not a problem since the Metsähovi station has mains power available.

The magnetometer used the same Raspberry Pi as the main board, but since the new sensors were analog, an external analog-to-digital converter (ADC) was needed. The MCP3424 was chosen for its ready availability in shield format for the RPi, low cost and good resolution of 18 bits (as compared to the output resolution of 12 bits of the previous sensor).

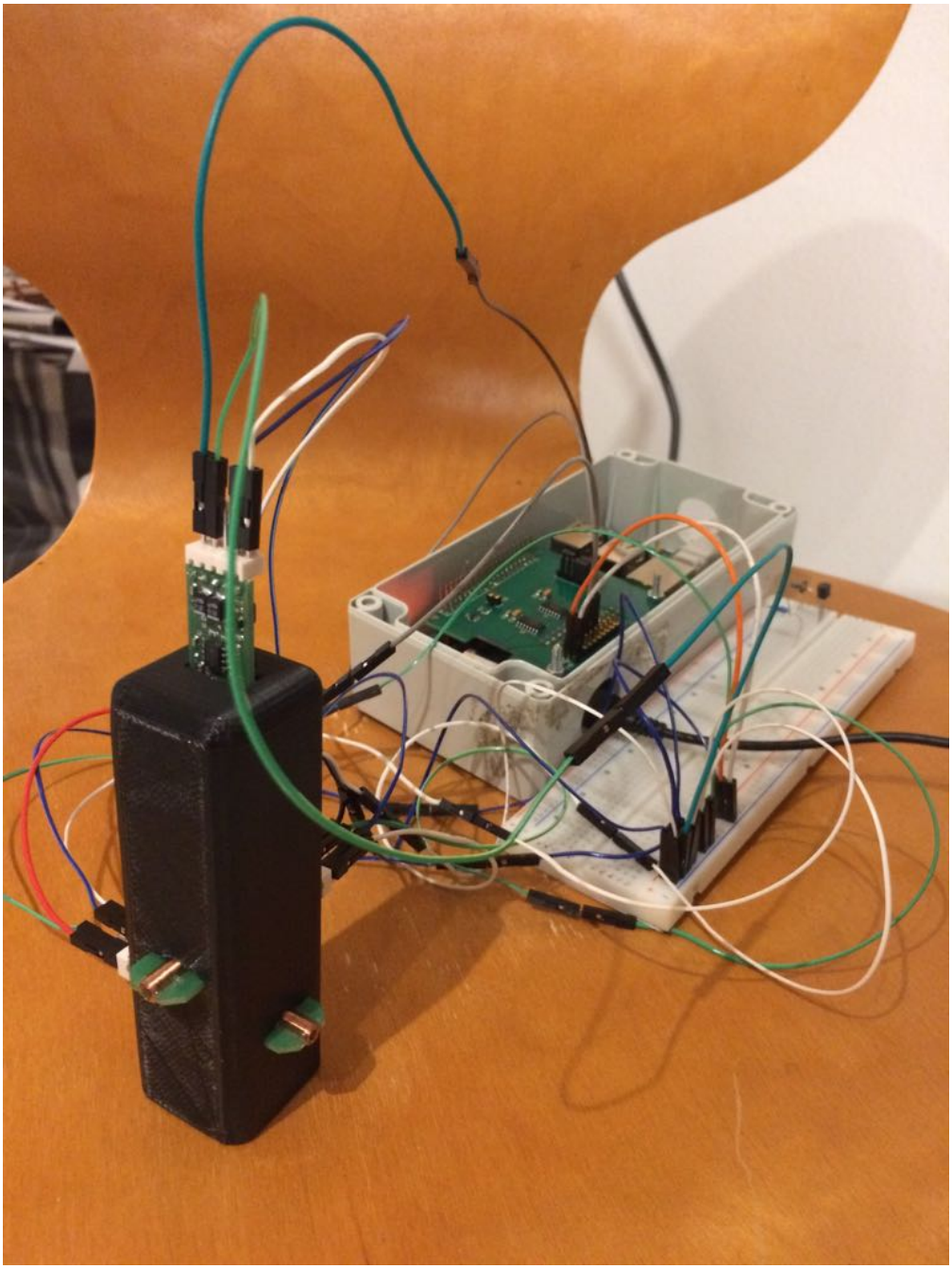

Figure 17: The improved Metsähovi magnetometer. On the left is the 3D printed sensor holder. The three sensors are partly visible, sticking out from different sides of the holder. In the back is the Raspberry Pi housing, equipped with a MCP3424 ADC. Picture courtesy of Joonas Viuho.

Figure 18: The improved magnetometer being installed at Metsähovi. The magnetometer was mounted on a tripod with a ball head for easy adjustment of orientation. Picture courtesy of Joonas Viuho.

Figure 19: The improved magnetometer with its plastic cover. Picture courtesy of Joonas Viuho.

5.6 CubeMAG

Aboard the ESTCube-1 satellite was a HMC5883L magnetometer used in the attitude control and determination system (ADCS) [42]. After the mission ended, the data collected by the magnetometer were analyzed. Some housekeeping data (rotational speeds, orientation among others) were used to remove the effects of the satellite's movement from the magnetic data. The magnetometer data show some geomagnetic activity. The measured geomagnetic field is shown in Fig. 20. The envelope wave of the oscillations of the field has a period of roughly 6 minutes or a frequency of 2.8 mHz, corresponding with Pc5 pulsations [8]. However, the resolution was not enough to pick up many significant transients in the geomagnetic field. Inspired by this, a magnetometer dedicated to scientific measurements was included in the ESTCube-2 mission. At the time of writing, the development of the instrument is still ongoing as the satellite will be launched in 2019. The new instrument - CubeMAG - will have several key improvements over the Metsähovi magnetometer. First of all, the new sensor produces an analog signal and has a much higher sensitivity than the HMC5883L. Combined with a high-resolution ADC, the resolution of the magnetometer is roughly 5 nanoteslas, two orders of magnitude better than the old Metsähovi magnetometer. The magnetometer will be controlled with a microcontroller that reads the digital data from the ADC and sends it to the on-board computer (OBC) of the satellite. The communication system then sends it to the ground station, after which the data can be analyzed.

The new sensor will be the HMC2003, produced by Honeywell [45]. The HMC2003 is actually a combination of two other sensors, HMC1001 and HMC1002. The previous is a 1-dimensional magnetoresistive vector magnetometer and the latter is a 2-dimensional magnetoresistive vector magnetometer. Combined, they form a 3D vector magnetometer capable of measuring the direction and the strength of the field. The output is analog and the sensitivity is 1 volt per 10000 nanotesla. In a null field, the sensor outputs 2.5 volts and this output is either increased or decreased linearly as a function of the field strength. The sensor accepts a range of supply voltages from 6 to 15 volts and demands up to 20 milliamperes of current. The power demand of the sensor is a bit on the high side for a CubeSat, but the combination of small footprint of 18.9x26.6x11.4 millimeters and good resolution makes the sensor a very good choice for a small satellite mission.

The analog signal of the sensor is digitized with an external ADC, ADS122U04 [46].

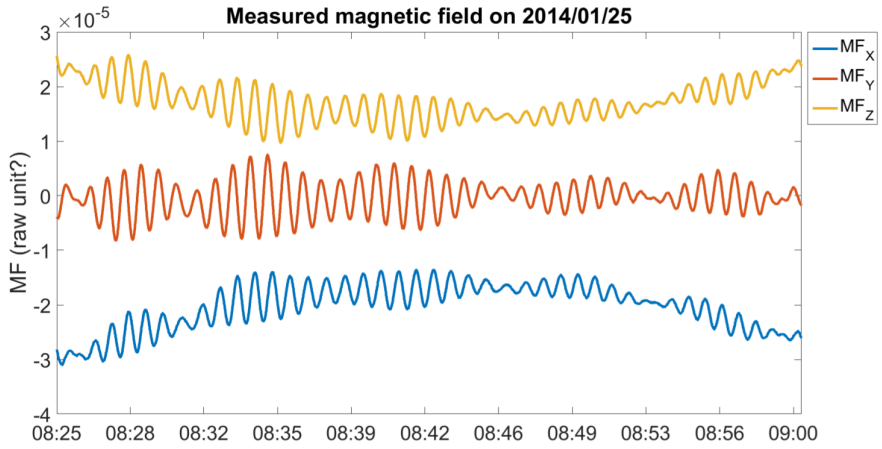

Figure 20: Magnetic data from the ESTCube-1 ADCS magnetometer. Despite the low resolution of 200 nT, the data show interesting features. The data presented here is orientation-corrected, so the oscillations in the data are caused by some external source, likely oscillations in the interplanetary magnetic field. The instrument was not calibrated for scientific measurements and thus the units are arbitrary. The orientation data used to correct the magnetic data is shown in Fig. 21. (Personal communication with Hendrik Ehrspais & Indrek Sünter)

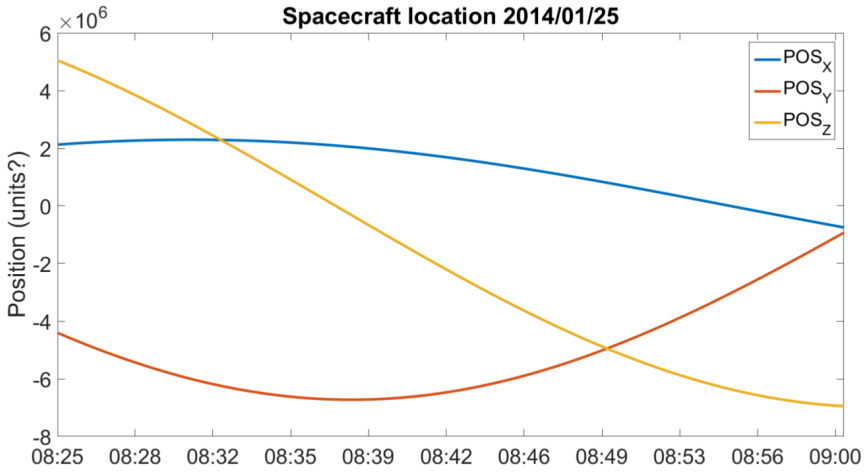

Figure 21: Orientation of the ESTCube-1 spacecraft. This orientation data is used to correct the raw magnetic data and remove any features caused by the orientation of the magnetometer. The data from magnetometer of the ESTCube-2 satellite will have to undergo a similar correction procedure. (Courtesy of the ESTCube team, especially Hendrik Ehrspais)

The ADC offers 24-bit resolution and sampling rates of up to 2000 samples per second, which is more than enough for the CubeMag. The power consumption of the ADC is also modest: the supply voltage is 5 volts and the current draw in the microampere range. Unfortunately the external ADC is not capable of parallel conversion of all channels at the same time, and thus needs to be reconfigured between conversions. This limits the output data rate to around 140 Hz which is comparable to the 160 Hz output data rate of the HMC5883L [39].

The sensor will be controlled by an STM32F100 microcontroller. The sensor will be placed on the same circuit board as the E-sail payload, so the same microcontroller will control both payloads. The microcontroller communicates with the ADC over serial UART and over a yet to be decided protocol with the on-board computer of the satellite. The microcontroller is programmed in C, using the Standard Peripheral Library provided by STMicroeletronics. The microcontroller is another major power sink in the system, requiring up to 15 milliamperes at 3.6 volts. However, the STM32F100 requires this much current only with all peripherals enabled. Disabling unnecessary features like the built-in ADC and DAC and utilizing low-power modes, the current consumption can be lowered below one milliampere.

The new, more sensitive magnetometer will also be much more sensitive to noise arising from the satellite itself. Some of these effects - so called hard-iron effects caused by the metallic structures of the satellite - can be mitigated with careful calibration, but others, like magnetic fields generated by current in the conductors of the satellite, are more difficult to predict and remove beforehand by calibration. Thus, before analysis, housekeeping data of the satellite will be needed to identify sources of transients of non-Solar origin. Also, since the satellite will be powered by solar panels, the magnetometer can mostly be used on the dayside of Earth to minimize battery usage and make sure that all critical subsystems of the satellite can function over the whole orbit. The satellite will also be equipped with several low resolution magnetometers for the ADCS. The data of these magnetometers will be used to correct for the position of the satellite in the data produced by CubeMAG.

The aim of the CubeMAG project is to show that science grade magnetometers can be placed onboard small and cheap CubeSats. The cost of a CubeSat project, including hardware, work hours and launch, is much smaller than the cost of a conventional full scale satellite. CubeSat budgets are often of the order of hundreds of thousands of

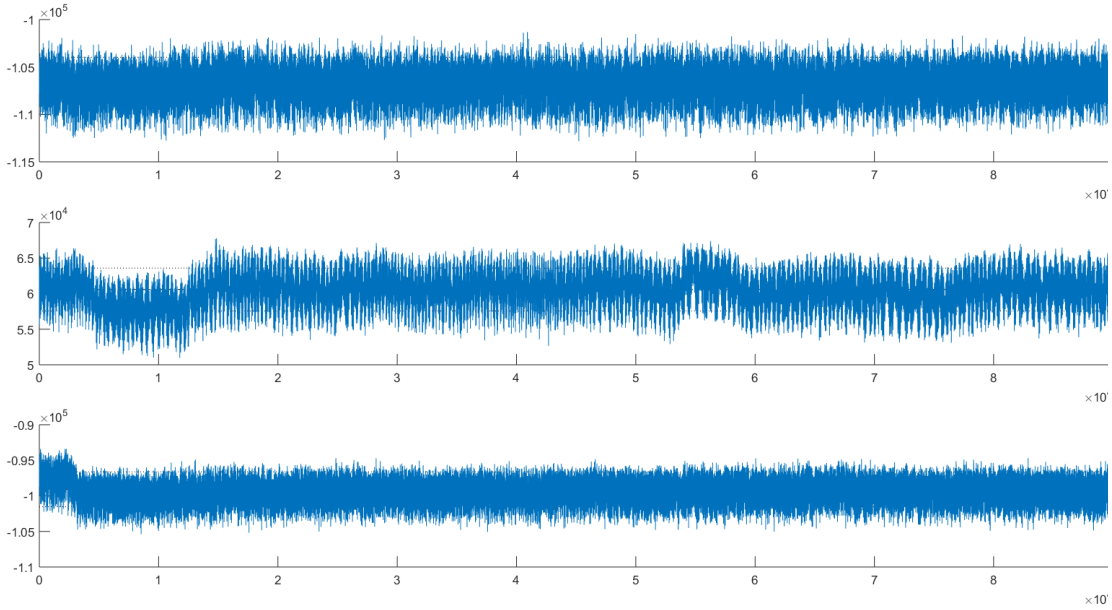

Figure 22: A test plot of the CubeMAG magnetometer. The magnetometer was uncalibrated and thus the units are not exactly nanoteslas, but they are of the correct magnitude.

euros, as opposed to full scale satellites budgets of up to hundreds of millions of euros. Usually satellite magnetometers are placed on long, extendable booms to avoid the noise sources discussed above, but this is often not possible on a CubeSat due to the large size of the folded boom. Some allow for a boom even on a CubeSat, but unfortunately the CubeMag was included in the ESTCube-2 project too late to accommodate for a boom in the design [47]. Thus an additional aim is to show that it is still possible to collect good quality data even without a boom. The data from the low resolution ADCS magnetometers will also be available and can be used to detect and correct for magnetic fields produced by the satellite electronics.

6 Future perspectives

To improve the performance of the Metsähovi magnetometer, some modifications are needed. First of all, the SD card of the Raspberry Pi quickly starts corrupting due to the frequent writing. SD cards are usually rated for 100000 write cycles [48]. Since the Raspberry Pi writes to the card once every second, the 100000 write cycle rating is

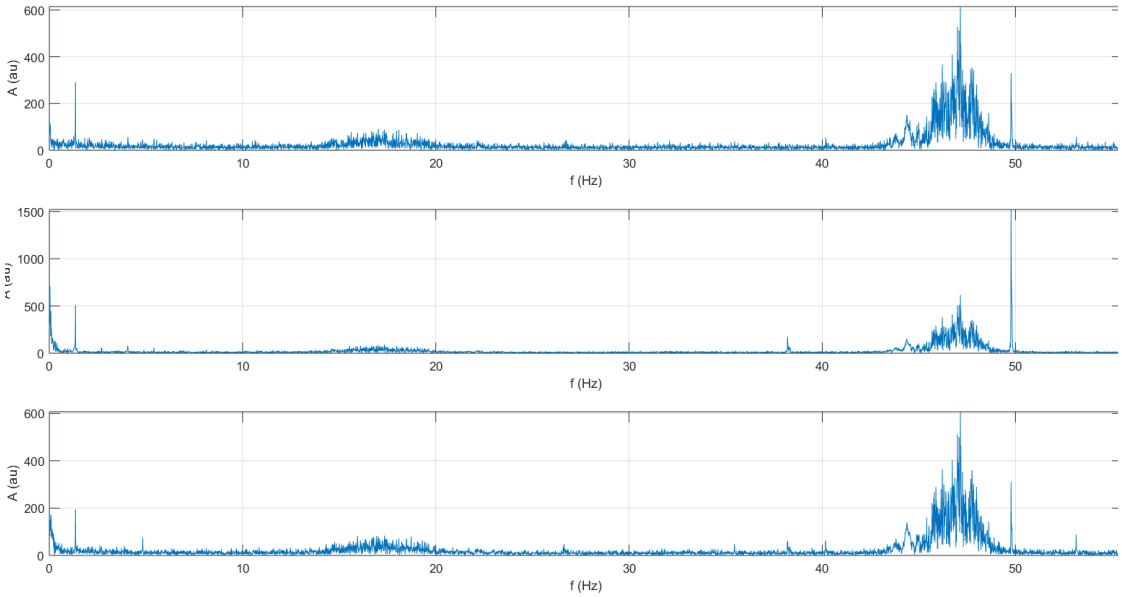

Figure 23: The frequency spectrum of the data in Fig. 22. The sampling frequency of the magnetometer is roughly 140 Hz, so the highest measurable frequency is around 70 Hz. On the right side, the 50 Hz peak from grid power is clearly visible.

very quickly reached, after which the SD card starts quicky degrading. A more durable medium, for example a magnetic hard drive is needed. This poses other problems, since a magnetic hard drive produces lots of interference in the measurements and thus needs to be placed sufficiently far away. This requires changes in the magnetometer structure. Also, the bearings and lubricants of the HDD must be capable of performing during both the Finnish winter and summer, with temperatures ranging from -30 to 30 degrees Celsius. Very few hard drives can take such changes in temperatures. While IC memory chips, like the AT24CM02 EEPROM memory, offer a large operating temperature range (-55 to 125 degrees Celsius) and a high number of write cycles (rated for 1000000 read/write operations), the provided storage space is too small: a standard SD card can store several gigabytes of data while an EEPROM chip can store a few megabytes.

The sensor of the magnetometer needs to be upgraded. The HMC5883L didn't pick up the interference from the movement of the satellite dish, so the resolution could well be improved. Also, a resolution of 200 nT can observe only the strongest disturbances of the geomagnetic field.

The resolution would be easiest to improve using an analog sensor and an external analog-to-digital converter. For example, the HMC2003 magnetoresistive sensor can reach an analog resolution of 4 nT [45]. Combined with a 16-bit ADC, the resultant digital resolution would be 5 nT, resulting in an improvement of 2 orders of magnitude in resolution with an increase of the order of 500 euros in price. This resolution would be able to detect most geomagnetic disturbances and provide good, scientific quality data. However, the choice of the ADC affects the measurement frequency. E.g. the MCP3424 ADC [49] achieves at most 240 samples per second. Taking into account the time needed to transmit the data, this sampling frequency could easily fall below 100 Hz. On the other hand, a higher-performance ADC like the ADS122U04 [46], can take up to 2000 samples per second. Accounting for data transmission times, the resulting sampling frequency is around 140 Hz for all three axes of the magnetic field. An example measurement of the magnetic field in a noisy, underground electronics laboratory is shown in Fig. 22 and a Fourier transform of the measurement in Fig. 23. The latter figure clearly shows a frequency range up to the Nyquist limit of the instrument, around 70 hertz. The 50 hertz mains power hum is clearly visible as a spike on the right hand side of the graph.

The infrastructure of the Metsähovi observatory provides reliable power and data connections for a magnetometer. However, the mounting of the magnetometers has to be

improved in the future. The original magnetometer was mounted on a wooden pole buried in the ground with a small section over the ground. Freezing and thawing of the ground moved the pole so the alignment of the magnetometer would not be precise enough for good measurements. This was not a significant problem with the first version, since it's aim was to see whether the large satellite dish created noise in the measurements and if the infrastructure was appropriate for a magnetometer. This may however be problematic for future versions. One solution would be to build a small hut with a concrete base. The hut would also serve as weather protection and would facilitate on-site maintenance, eg. changing sensors or storage devices if needed.

Completely infrastructure-independent operation may be achieved by changing the controller and sensors. Normal operation of the RPi requires 5 volts and up to 1 ampere during normal operation. By switching the RPi to a low-power microcontroller, like the STM32L1 and the sensor to a higher quality magnetometer, eg. STMicroelectronics LIS3MDL, the magnetometer can be powered by a battery instead of mains power. Both can be operated with a low supply voltage of 3.3 volts, and consume very little power: the STM32L1 microcontroller requires 8.6 microamperes in low-power mode and the LIS3MDL may operate with as little as 40 microamperes. Thus, assuming a 50 % depth of discharge, a typical lithium-ion battery cell with a capacity of 2500 milliampere-hours [50] could ideally power the controller and the sensor for over 25000 hours or well over 2 years. Of course, the data has to be recorded in some way. One way around the limitations of solid state recording devices is to use, for example, an off-the-shelf GSM module to allow wireless data transfer over the cellphone network. Such modules are readily available (eg. SIMCom SIM900D [51]). The SIM900D requires the same 3.3 volts that powers the controller and the sensor, but requires higher currents: 1 milliampere during standby mode and up to 2 amperes during transmission. Depending on data packing and strength of the GSM network signal, the transmission periods may be very short, but nonetheless may significantly affect the battery life of the wireless instrument.

The lessons learned during this project can be applied to other instruments. Not too many science grade magnetometers have been launched to the orbit, so there is not too much data about the geomagnetic field in space. Usually magnetometers aboard satellites require the magnetometer to be mounted on a boom several meters in length to minimize the magnetic effect of the satellite on the sensor. However, on ESTCube-1 there was a HMC5883L used for attitude determination [42]. The data was later analyzed to see if the magnetometer was able to observe disturbances in the geomagnetic

field. ESTCube-2 will be equipped with a higher-resolution HMC2003 magnetometer dedicated for scientific measurements and not just attitude control. Aalto-3, a Finnish CubeSat will carry a science grade magnetometer built from COTS components and other satellite missions (for example ESTCube-3) may also be equipped with one.

7 Discussion and summary

These magnetometers have been proof-of-concept designs. The aim of this project was to see if it is possible to place an affordable autonomous magnetometer at Metsähovi. One unanswered question was how accurate a magnetometer can be placed at the vicinity of the radio telescope without getting too much interference in the measurements. With the HMC5883L, no interference was seen in the data. Some very strong geomagnetic disturbances, however, were observed. This means that the HMC5883L could be replaced with a higher-resolution sensor without significant interference from the radio telescope while also keeping the budget relatively low, at least compared to the price of a e.g. LEMI-025 or SFGE.

A low-cost science grade magnetometer CubeMAG was also designed to be launched into the orbit aboard the ESTCube-2 nanosatellite. The development of the instrument is still ongoing, but lessons learned from the process are very valuable in improving the design of Earth-based magnetic instruments.

Current commercial technology certainly allows launching campaigns similar to the Scandinavian Magnetometer Array, but the cost of state-of-the-art instruments may be prohibitingly high. The combined efforts of the described projects enable production of magnetometers with sufficient performance at a fraction of the cost. Such a drop in costs may make a "new Scandinavian Magnetometer Array" a feasible possibility, with the added benefit of digital instruments allowing skipping the digitization process completely and enabling automatic analysis of data.

References

[1] William Lowrie. *Fundamentals of Geophysics*. Cambridge University Press, 2007.

[2] L. Bolduc. GIC observations and studies in the Hydro-Québec power system. *Journal of Atmospheric and Solar-Terrestrial Physics*, 64:1793–1802, November 2002. doi: 10.1016/S1364-6826(02)00128-1.

[3] Louis J. Lanzerotti. *Space Weather Effects on Technologies*, pages 11–22. American Geophysical Union (AGU), 2013. ISBN 9781118668351. doi: 10.1029/GM125p0011. URL `https://agupubs.onlinelibrary.wiley.com/doi/abs/10.1029/GM125p0011`.

[4] Heikki Nevanlinna. Geomagnetismin ABC-kirja. Technical report, Ilmatieteen laitos, 2009.

[5] R.P. Lepping, D.B. Berdichevsky, C.-C. Wu, A. Szabo, T. Narock, F. Mariani, A.J. Lazarus, A.j: Quivers. A summary of WIND magnetic clouds for years 1995–2003: model-fitted parameters, associated errors and classifications. *Annales Geophysicae*, 24:215–245, 2006.

[6] E.I. Tanskanen. A comprehensive high-throughput analysis of substorms observed by IMAGE magnetometer network: Years 1993–2003 examined. *Journal of Geophysical Research*, 114, 2009.

[7] E.I. Kallio, T.I. Pulkkinen, H.E.J. Koskinen, A. Viljanen, J.A. Slavin, and K. Ogilvie. Loading-unloading processes in the nightside ionosphere. *Geophysical Research Letters*, 27(11):1627–1630, 2000.

[8] Takao Saito. Geomagnetic pulsations. *Space Science Reviews*, 10, 1969.

[9] William Gilbert. *De Magnete*. Peter Short, 1600.

[10] Sidney Chapman and Julius Bartels. *Geomagnetism, volume I*. Oxford University Press, 1940.

[11] Sidney Chapman and Julius Bartels. *Geomagnetism, volume II*. Oxford University Press, 1940.

[12] J.A. Jacobs. *Geomagnetism, vol. I*. Academic Press, 1987.

[13] Merrill, Ronald T. *The Earth's Magnetic Field: Its History, Origin, and Planetary Perspective.* Number v. 32 in International Geophysics Series. Academic Press, 1983. URL http://search.ebscohost.com/login.aspx?direct=true&db=nlebk&AN=297129&site=ehost-live&scope=site.

[14] Carl Friedrich Gauss. The Intensity of the Earth's Magnetic Force Reduced to Absolute Measurement. http://21stcenturysciencetech.com/translations/gaussMagnetic.pdf, 1832.

[15] F. Küppers and H. Post. A Second Generation Gough-Reitzel Magnetometer. *Journal of geomagnetism and geoelectricity*, 33(3):225–237, 1981. doi: 10.5636/jgg.33.225.

[16] William Thomson. On the Electro-Dynamic Qualities of Metals:–Effects of Magnetization on the Elextric Conductivity of Nickel and of Iron. *Proc. R. Soc. Lond.*, 8 (XIX), 1856.

[17] Janice Nickel. Magnetoresistance overview. Technical report, 1995.

[18] P.W. Bridgman. Biographical Memoir of Edwin Herbert Hall. *Biographical Memoirs of the National Academy of Sciences*, XXI(2), 1939.

[19] Robert C. Snare. *A History of Vector Magnetometry in Space.* American Geosciences Union, 1998.

[20] Lviv Centre of Institute of Space Research. Intermagnet 1-second standard flux-gate magnetometer LEMI-025 user manual, revision 1.4.

[21] Alexei Gvishiani, Renata Lukianova, Anatoly Soloviev, and Andrei Khokhlov. Survey of geomagnetic observations made in the northern sector of russia and new methods for analysing them. *Surveys in Geophysics*, 35(5):1123–1154, Sep 2014.

[22] L. Häkkinen H. Nevanlinna. Results of Russian geomagnetic observatories in the 19th century:magnetic activity, 1841–1862. *Annales Geophysicae*, 28:917–926, 2010.

[23] Alexei Gvishiani, Renata Lukianova, Anatoly Soloviev, and Andrei Khokhlov. Survey of Geomagnetic Observations Made in the Northern Sector of Russia and New Methods for Analysing Them. *Surveys in Geophysics*, 35(5):1123–1154, Sep 2014.

[24] Heikki Nevanlinna. *Kaisaniemestä Kumpulaan - tutkimusta, havaintoa ja ihmisiä Ilmatieteen laitoksessa.* Yliopistopaino, 2005.

[25] University of Oulu. SOD Geomagnetic Observatory. http://www.sgo.fi/Data/Magnetometer/magnetometer.php. [Retrieved 2.12.2018].

[26] Finnish Meteorological Institute. Geomagneettiset aikavaihtelut observatoriorekisteröintien mukaan. http://www.ava.fmi.fi/MAGN/HN/gmg08_06.pdf, . [Lecture series on geomagnetism by the Finnish Meteorological Institute; Retrieved 31.3.2016].

[27] INTERMAGNET. List of IMOs and Responsible GINs. http://www.intermagnet.org/imos/imotblobs-eng.php. [Retrieved 2.12.2018].

[28] Finnish Meteorological Institute. IMAGE-magnetometriverkosto. http://space.fmi.fi/image/beta/?page=maps, . [Retrieved 4.4.2016].

[29] Beverly F. Ronalds. The Beginnings of Continuous Scientific Recording using Photography: Sir Francis Ronalds' Contribution. http://www.eshph.org/wp-content/uploads/2016/05/ronalds_camera.pdf, 2016. Retrieved 15.9.2016.

[30] J. S. Reitzel D.I. Gough. A portable three-component magnetic variometer. *Journal of geomagnetism and geoelectricity*, 19(3):203–215, 1967. doi: 10.5636/jgg.19.203.

[31] Kari Pajunpää. Geomagnetic observations (instrumentation, calibration, data processing). www.spaceclimate.fi/SC6/lectures/KariPajunpaa.pdf, 2016.

[32] Swedish Institute of Space Physics. Flux-gate magnetometer. http://www2.irf.se/Observatory/flux.gif. [Retrieved 26.3.2019].

[33] R. I. Potter T. R. McGuire. Anisotropic magnetoresistance in ferromagnetic 3d alloys. *IEEE transactions on magnetics*, 11(4), 1975.

[34] J. Untiedt and W. Baumjohann. Studies of polar current systems using the ims scandinavian magnetometer array. *Space Science Reviews*, 63(3):245–390, Sep 1993.

[35] NIPR Symposium on Upper Atmosphere Physics. and Kokuritsu Kyokuchi Kenkyujo (Japan). Proceedings of the nipr symposium on upper atmosphere physics, 1988. ISSN 0914-5613.

[36] G. Marklund, I. Sandahl, and H. Opgenoorth. A study of the dynamics of a discrete auroral arc. *Planetary and Space Science*, 30(2):179 – 197, 1982. ISSN 0032-0633. doi: https://doi.org/10.1016/0032-0633(82)90088-5. URL http://www.sciencedirect.com/science/article/pii/0032063382900885.

[37] Raspberry Pi Foundation. Raspberry Pi 2 Model B product page, . https://www.raspberrypi.org/products/raspberry-pi-2-model-b/; retrieved on 10.10.2016.

[38] Adafruit. Raspberry pi 2 model b product page. https://www.adafruit.com/product/2358; retrived on 10.10.2016.

[39] *3-Axis Digital Compass IC*. Honeywell Inc., 2013.

[40] Danish National Space Institute. 3-axis Fluxgate Magnetometer Model FGE. http://www.space.dtu.dk/English/Research/Instruments_Systems_Methods/3-axis_Fluxgate_Magnetometer_Model_FGM-FGE.aspx, . [Product page for DTU's SFGE magnetometer; retrieved 25.4.2016].

[41] Raspberry Pi Foundation. SALES SOAR AND RASPBERRY PI BEATS COMMODORE 64, . https://www.raspberrypi.org/magpi/raspberry-pi-sales/; retrieved on 4.11.2018.

[42] *Attitude determination and control for centrifugal tether deployment on the ESTCube-1 nanosatellite*, volume 63 of *2S*, 2014. Estonian Academy Publishers.

[43] Guowen Sun and Xiwang Xia and Shufan Wu and Ziyi Wu and Wen Chen and Zhao Li. Attitude Determination and Control System Design for STU-2A Cubesat and In-Orbit Results, 2016. Retrieved 12.4.2018, https://digitalcommons.usu.edu/cgi/viewcontent.cgi?article=3466&context=smallsat.

[44] *Magnetic Field Sensor FLC 100*. Stefan Mayer Instruments.

[45] *3-Axis Magnetic Sensor Hybrid HMC2003*. Honeywell Inc., 2011.

[46] *ADS122U04 24-Bit, 4-Channel, 2-kSPS, Delta-Sigma ADC With UART Interface*. Texas Instruments.

[47] Celena Dopart, Robert Morlath, Erik Oliver, and Jake Schomaker. Design And Analysis for a CubeSat Mission. Master's thesis, Worcester Polytechnic Institute, 2012.

[48] *SanDisk Secure Digital Card Product Manual*. SanDisk Corporation, 2003.

[49] *18-Bit, Multi-Channel $\Delta\Sigma$ Analog-to-Digital Converter with I2C Interface and On-Board Reference*. Microchip.

[50] *INR18650-25R*. Samsung SDI CO., Ltd., 2014.

[51] *SIM900D Hardware Design*. Shanghai SIMCom Wireless SOlutions Ltd., 2012.